Nucleic Acids Research, 2023, **51**, 10950–10969
https://doi.org/10.1093/nar/gkad763
Advance access publication date: 9 October 2023
Gene regulation, Chromatin and Epigenetics

An interaction between eIF4A3 and eIF3g drives the internal initiation of translation

Jeeyoon Chang[1,†], Min-Kyung Shin[2,†], Joori Park[2,†], Hyun Jung Hwang[1], Nicolas Locker[3], Junhak Ahn[4], Doyeon Kim[4], Daehyun Baek[4], Yeonkyoung Park[1], Yujin Lee[2], Sung Ho Boo[2], Hyeong-In Kim[1] and Yoon Ki Kim[1,*]

[1]Department of Biological Sciences, Korea Advanced Institute of Science and Technology, Daejeon 34141, Republic of Korea
[2]Division of Life Sciences, Korea University, Seoul 02841, Republic of Korea
[3]Department of Microbial and Cellular Sciences, University of Surrey, Guildford GU2 7HX, UK
[4]School of Biological Sciences, Seoul National University, Seoul 08826, Republic of Korea

[*]To whom correspondence should be addressed. Tel: +82 42 350 7927; Email: yk-kim@kaist.ac.kr
[†]These authors contributed equally to this work.

Abstract

An RNA structure or modified RNA sequences can provide a platform for ribosome loading and internal translation initiation. The functional significance of internal translation has recently been highlighted by the discovery that a subset of circular RNAs (circRNAs) is internally translated. However, the molecular mechanisms underlying the internal initiation of translation in circRNAs remain unclear. Here, we identify eIF3g (a subunit of eIF3 complex) as a binding partner of eIF4A3, a core component of the exon-junction complex (EJC) that is deposited onto spliced mRNAs and plays multiple roles in the regulation of gene expression. The direct interaction between eIF4A3-eIF3g serves as a molecular linker between the eIF4A3 and eIF3 complex, thereby facilitating internal ribosomal entry. Protein synthesis from *in vitro*-synthesized circRNA demonstrates eIF4A3-driven internal translation, which relies on the eIF4A3-eIF3g interaction. Furthermore, our transcriptome-wide analysis shows that efficient polysomal association of endogenous circRNAs requires eIF4A3. Notably, a subset of endogenous circRNAs can express a full-length intact protein, such as β-catenin, in an eIF4A3-dependent manner. Collectively, our results expand the understanding of the protein-coding potential of the human transcriptome, including circRNAs.

Graphical abstract

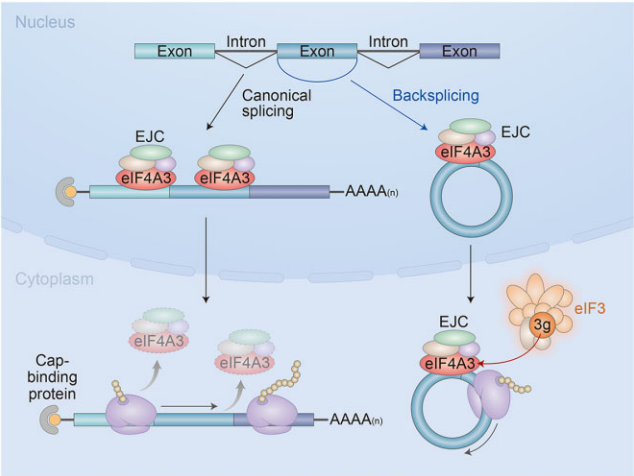

Introduction

In eukaryotic cells, translation initiation is a pivotal stage in gene regulatory pathways (1,2). In conventional cap-dependent translation, the 5′-cap structure of the messenger RNAs (mRNAs) plays a crucial role in ribosome recruitment to initiate translation. The cap structure is primarily recognized by one of two cap-interacting proteins: the nuclear cap-binding protein complex, which is a heterodimer of CBP80 and CBP20, and cytoplasmic eukaryotic translation initiation factor (eIF) 4E (3,4). Both cap-interacting proteins have the common ability to recruit the small subunit (40S) of the ribosome via eIF3. The recruited 40S ribosome scans the

Received: November 4, 2022. **Revised:** August 30, 2023. **Editorial Decision:** August 31, 2023. **Accepted:** September 8, 2023

5′ untranslated region (5′UTR) to search for an initiation codon in the proper nucleotide sequence context. When the 40S ribosome reaches the initiation codon, the large subunit (60S) of the ribosome joins to initiate protein synthesis.

Among the eIFs, eIF3 is the largest complex, consisting of 12 polypeptides (eIF3a-i and eIF3k-m) and plays multiple roles in translation (1,2,5–8). During the initiation step, eIF3 promotes the assembly of the pre-initiation complex, loading of the 40S ribosome onto the 5′-end of the mRNA, ribosome scanning along the 5′UTR and AUG recognition in the proper context. In addition to its role in translation initiation, eIF3 can interact with the translating 80S ribosome and affect the elongation and termination steps of translation, as well as ribosome recycling.

As an alternative to cap-dependent ribosome recruitment, internal ribosome entry sites (IRESes) located in the 5′UTR of a subset of cellular and viral mRNAs can provide a platform for ribosome loading and internal translation initiation (2,9). Recent studies have also shown that in addition to IRES, N^6-methyladenosine (m^6A; the most abundant internal modification in mRNAs) within the 5′UTR directs cap-independent translation via eIF3 recruitment (10).

The functional importance of internal translation was recently highlighted by the identification of a large number of circular RNAs (circRNAs), most of which are generated by the back-splicing of internal exons (11–13). Notably, a subset of circRNAs is translated internally (14–24). Although the emerging molecular functions of circRNAs include regulation of transcription, pre-mRNA splicing, mRNA stability and mRNA translation (25–27), the molecular mechanisms underlying the internal initiation of translation in circRNAs remain unclear (17,28).

The translation of newly synthesized mRNAs is regulated by an exon junction complex (EJC) that is deposited onto mRNAs ∼20–24 nucleotides upstream of exon–exon junctions as a consequence of a splicing event (29–31). The EJC is organized around the central core of four proteins with several peripheral proteins that clamp the RNA sequence. The core EJC is composed of eIF4A3, metastatic lymph node 51 (MLN51; also known as barentsz or CASC3), Y14 (also known as RNA-binding motif 8A) and the Mago-Nashi homolog (MAGOH). eIF4A3 is a member of the DEAD-box RNA helicase family that contains two globular domains (RecA1 and RecA2) involved in RNA binding and ATP hydrolysis. The two globular domains of eIF4A3 remain in an open structure and move freely in the absence of ATP. However, in the presence of ATP, eIF4A3 undergoes a conformational change and forms a closed structure that binds to RNA. MAGOH and Y14, which form a tight heterodimer, make contact with eIF4A3, blocking conformational changes and maintaining the RNA-bound form of eIF4A3. Additionally, MLN51 directly interacts with MAGOH and stabilizes both the open and closed structures of eIF4A3, thereby contributing to the stabilization of the EJC. In general, intron-containing mRNAs (i.e. mRNAs that undergo splicing) are translated more efficiently than intronless mRNAs with identical nucleotide sequences (32,33). In addition, following insulin treatment, the translation of intron-containing mRNAs is selectively promoted compared to that of their intronless counterparts (34). This preference is attributable in part to the EJC, which is deposited as a result of splicing, rather than to splicing *per se*.

This study provides molecular evidence supporting the internal initiation of translation driven by the interaction between eIF4A3 and eIF3g, highlighting a previously unknown layer of post-transcriptional regulation of gene expression.

Materials and methods

Cell lines

HeLa (female; ATCC), human embryonic kidney 293T (HEK293T) (fetal; ATCC), Huh7 (male; Korean Cell Line Bank), A549 (male; ATCC), U2OS (female; ATCC) and HepG2 (male; ATCC) cell lines were maintained in Dulbecco's modified Eagle's medium (DMEM; Capricorn Scientific) supplemented with 10% (v/v) fetal bovine serum (Capricorn Scientific) and 1% (v/v) penicillin/streptomycin solution (Capricorn Scientific) at 37°C and 5% CO_2. Stable HeLa cell lines expressing siRNA-resistant and doxycycline (Dox)-inducible FLAG-tagged eIF4A3-wild-type (WT) have been described previously (35). To induce FLAG-eIF4A3, 400 ng/ml Dox (MilliporeSigma) was added to the medium. To eliminate mycoplasma contamination, all cell lines were regularly treated with Plasmocin™ (Invitrogen) and tested using the MycoAlert PLUS Mycoplasma Detection Kit (Lonza). When indicated, the cells were washed four times with phosphate-buffered saline (PBS) and cultured in serum-free DMEM for 24 h before harvesting.

Plasmid construction

The following plasmids have been previously described or obtained elsewhere: pEBG (36); pRβ-SL87.8-Norm, pRSET-A-eIF4A3, p3 × FLAG-eIF4A3, which encodes human *eIF4A3* mRNA resistant to *eIF4A3* siRNA and p3 × FLAG-eIF4A3-(E188Q) (37); pcDNA-F/BoxB/R, pGEX-6p-1 + NdeI, pGEX-eIF3g and pcDNA3-FLAG-eIF3g (38); pCI-FLuc, pλN-HA and pλN-HA-GFP (39); PB-CuO-V5-CASC3 (Addgene; #158540); pCMV-MYC and pRSET-A (Clontech); pCMV-MYC-GST (40); pCMV-MYC-4E-BP1 (41); p3 × FLAG (MilliporeSigma); pλN-HA-Y14, pλN-HA-MAGOH, p3 × FLAG-eIF4A3-T163A and p3 × FLAG-eIF4A3-T163D (35); pCIRC-FP-IRES-G (42); pGL3-control (Promega); pRL-CMV (Promega); pBluescripts SK(-) and TOPFlash and FOPFlash (43).

To construct plasmid pEBG-eIF4A3, which expresses glutathione *S*-transferase (GST)-tagged full-length human eIF4A3, a Klenow-filled BglII/XbaI fragment of p3 × FLAG-eIF4A3 was ligated into a Klenow-filled NotI fragment of pEBG.

To generate plasmid pEBG-eIF3g-WT, a DNA fragment containing human *eIF3g* cDNA was amplified by PCR using pcDNA3-FLAG-eIF3g as a template and two specific oligonucleotides: eIF3g-F and eIF3g-R (Supplementary Table S1A). The PCR product was ligated into the BamHI/KpnI fragment of pEBG.

For the construction of plasmids pEBG-eIF3g (region 62–320), pEBG-eIF3g (region 151–320) and pEBG-eIF3g (region 232–320), the corresponding regions were amplified by PCRs from pcDNA3-FLAG-eIF3g as a template with specific oligonucleotides: eIF3g-F1 (sense for region 62–320), eIF3g-F2 (sense for region 151–320) or eIF3g-F3 (sense for region 232–320) and eIF3g-R (antisense for all; Supplementary Table S1A). For the construction of plasmids pEBG-eIF3g (region 151–186) and pEBG-eIF3g (region 151–231), the corresponding regions of human *eIF3g* cDNA were amplified by PCRs using pcDNA3-FLAG-eIF3g as a template and specific

oligonucleotides: eIF3g-F2 (sense for all), eIF3g-R1 (antisense for region 151–186) and eIF3g-R2 (antisense for region 151–231; Supplementary Table S1A). Each PCR product was ligated into the BamHI/KpnI fragment of pEBG.

For the bacterial production of 6× His-tagged human full-length eIF3g, a region containing human *eIF3g* cDNA was amplified by PCR from pcDNA3-FLAG-eIF3g as a template with two specific oligonucleotides: eIF3g-recomb-F and eIF3g-recomb-R (Supplementary Table S1A). The PCR product was ligated into the XhoI/KpnI fragment of pRSET-A.

To construct the pGEX-eIF4A3 plasmid, which produces GST-fused human eIF4A3 in a bacterial system, a DNA fragment containing human *eIF4A3* cDNA was amplified by PCR using p3 × FLAG-eIF4A3 as the template and two specific oligonucleotides: eIF4A3-recomb-F and eIF4A3-recomb-R (Supplementary Table S1A). The PCR product was ligated into the BamHI/XhoI fragment of pGEX-6p-1 + NdeI.

To construct pλN-HA-eIF4A3-WT, -T163A or -T163D, the Klenow-filled ClaI/XbaI fragment of p3 × FLAG-eIF4A3-WT, -T163A or -T163D was ligated to the Klenow-filled EcoRI/XbaI fragment of pλN-HA, respectively.

For the construction of pλN-HA-eIF4A3-E188Q, an EcoRV fragment of p3 × FLAG-eIF4A3-E188Q harboring a mutation was ligated to an EcoRV fragment of pλN-HA-eIF4A3-WT.

To construct pλN-HA-eIF4A3-D154K/Y155A and -D401K/E402R, which cannot bind to MNL51 and the Y14/MAGOH heterodimer, respectively, the corresponding region in pλN-HA-eIF4A3-WT was replaced with each fragment of *eIF4A3* cDNA harboring substitutions D154K/Y155A or D401K/E402R (Supplementary Table S1A).

To generate pλN-HA-MLN51, a DNA fragment containing human *MLN51* cDNA was amplified by PCR using PB-CuO-V5 CASC3 as the template and two specific oligonucleotides, MLN51-F and MLN51-R (Supplementary Table S1A). The PCR product was ligated into the EcoRI/NotI fragment of pλN-HA-eIF4A3-WT.

To generate plasmid pλN-HA-eIF3g, a DNA fragment containing human *eIF3g* cDNA was amplified by PCR using pcDNA3-FLAG-eIF3g as a template and two specific oligonucleotides, eIF3g-F4 and eIF3g-R3 (Supplementary Table S1A). The PCR product was ligated into the EcoRI/NotI fragment of pλN-HA-eIF4A3-WT.

To construct p3 × FLAG-eIF4A3-D154K/Y155A and -D401K/E402R, the AccI/XbaI fragment of p3 × FLAG-eIF4A3-WT was ligated into the AccI/XbaI fragments of pλN-HA-eIF4A3-D154K/Y155A and -D401K/E402R, respectively.

For artificial tethering of eIF4A3 or its variants to the 5′UTR of *renilla* luciferase gene (RLuc) mRNA, the pcDNA3-SL-BoxB-R plasmid, which contains both a strong stem-loop structure (SL) and 12 tandem repeats of BoxB in the 5′UTR, was constructed by inserting the SL and a PCR-amplified BoxB sequence into the 5′UTR of the RLuc gene. First, SL-containing fragments were obtained from a NheI/NcoI-digested fragment of pRβ-SL87.8-Norm. Second, the 12BoxB-containing sequence was amplified from pcDNA-F/BoxB/R using two oligonucleotides, 12BoxB-F and 12BoxB-R (Supplementary Table S1A). The resulting PCR products were digested with NcoI and BstB1. Finally, the SL and PCR-amplified BoxB sequences were ligated to the linearized pcDNA-F/BoxB/R digested with NheI and BstB1. To construct pcDNA3-BoxB-R, the HindIII-digested fragment of pcDNA3-SL-BoxB-R was self-ligated.

To generate plasmids, pλN-HA-eIF1, -eIF3i and eIF5, DNA fragments containing human *eIF1*, *eIF3i* and *eIF5* cDNAs were purchased from Korea Human Gene Bank (BKU006023, BKU006981 and hMU008661). cDNAs were amplified by PCR using two specific oligonucleotides: eIF1-F and eIF1-R, eIF3i-F and eIF3i-R, and eIF5-F and eIF5-R (Supplementary Table S1A). PCR products were ligated into the XbaI/NotI fragment of pλN-HA-GFP.

Dicistronic reporter plasmids Gl1 and Gl3, with or without the β-globin intron, were constructed by a series of PCRs. A DNA fragment containing the β-globin intron was obtained by PCR, using pcDNA3.1-cβGl-Norm-8bs as the template. The nucleotide sequences corresponding to the intercistronic regions of the resulting Gl1 and Gl3 plasmids are listed in Supplementary Table S2A. Plasmids Gl2 and Gl4, which contain a strong SL in the 5′UTR, were constructed by inserting the SL-containing fragment of pRβ-SL87.8-Norm into the 5′UTR of Gl1 and Gl3, respectively.

To construct pSK-Circ-BoxB-R for the generation of *in vitro*-transcribed Circ-BoxB-R, sequences containing a group I self-splicing intron (44), 12 tandem repeats of BoxB and the *RLuc* gene were synthesized *in vitro* (Integrated DNA Technologies). Next, the *in vitro*-synthesized fragment was ligated to the PvuII fragment of pBluescript SK(−). The pSK-Circ-R plasmid was generated by the self-ligation of the EcoRI fragment of pSK-Circ-BoxB-R (Supplementary Table S2B).

To construct plasmids FLAG-cCTNNB1s encoding FLAG-tagged circRNAs of the *CTNNB1* gene, the DNA fragments corresponding to cCTNNB1a, cCTNNB1b and cCTNNB1c were amplified by PCR using cDNA from HeLa cells as a template and specific oligonucleotides (Supplementary Table S1A): cCTNNB1-F (sense for all), cCTNNB1a-R (antisense for cCTNNB1a), cCTNNB1b-R (antisense for cCTNNB1b) and cCTNNB1c-R (antisense for cCTNNB1c), respectively. Next, the nucleotide region of green fluorescent protein (GFP) in pCIRC-FP-IRES-G was replaced with the amplified PCR products. Finally, a nucleotide sequence encoding the FLAG peptide was inserted immediately downstream of the putative translation initiation codon (Supplementary Table S2C).

PCR amplification was performed using the Advantage-HF2 PCR Kit (Clontech), following the manufacturer's instructions. All constructs were verified by DNA sequencing.

DNA or siRNA transfection

Cells were transiently transfected with (i) various plasmids using either Lipofectamine 2000 (Life Technologies) or TurboFect (Thermo Fisher Scientific) or (ii) 100 μM *in vitro*-synthesized siRNAs (GenePharma) using either Oligofectamine (Life Technologies) or Lipofectamine 3000 (Life Technologies) as previously described (35,36,40,45). The calcium phosphate transfection method was used for immunoprecipitation (IP) and RNA-IP experiments on HEK293T cells. The siRNAs used in our study are listed in Supplementary Table S1B along with references (46–48).

The yeast two-hybrid assay

This screening was performed by PanBioNet, Inc. (Pohang, Republic of Korea) using GAL4 BD-eIF4A3 and an AD-fused human thymus cDNA library (Clontech). Specific interactions

between eIF4A3 and AD-eIF3 subunits were also confirmed using a yeast two-hybrid assay (PanBioNet Inc.).

IP, RNA-IP and the glutathione-*S*-transferase pull-down assay

IP, glutathione-*S*-transferase (GST) pull-down assays and RNA-IP were performed as previously described (35,36,40). For the IP, cells were washed once with ice-cold PBS and harvested, followed by centrifugation at 3000 × *g* for 10 min at 4°C. The cell pellet was resuspended in 500 μl of NET-2 buffer [50 mM Tris-HCl (pH 7.4), 150 mM NaCl, 1 mM phenylmethylsulfonyl fluoride (PMSF), 2 mM benzamidine hydrochloride and 0.05% Nonidet P-40] and sonicated twice with 30 bursts of 1 s each (output control: 3, duty cycle: 30%; Sonifier 250, Branson). After centrifugation at 13 000 × *g* for 10 min at 4°C, the supernatant was precleared by incubation with 50 μl of Protein G Agarose 4B (Incospharm) for 1 h at 4°C. The precleared supernatants were incubated for 3 h at 4°C with either antibody-conjugated beads or FLAG M2 affinity gel (Millipore, Sigma). Next, the beads were washed five times with NET-2 buffer and resuspended in 100 μl of 2 × sample buffer [1.43 M β-mercaptoethanol, 4% (w/v) sodium dodecyl sulfate (SDS), 125 mM Tris-HCl (pH 6.8), 15% (v/v) glycerol and 0.01% bromophenol blue]. Co-immunoprecipitated proteins were analyzed using western blotting.

RNA-IP was conducted similarly to IP, except that (i) NET-2 buffer was supplemented with 0.2 U/μl RiboLock RNase inhibitor (Thermo Fisher Scientific), (ii) the beads were saturated with 6.7 μg/μl denatured yeast tRNAs (MilliporeSigma) before mixing with the precleared lysate and (iii) the bound RNAs were extracted with phenol/chloroform/isoamyl alcohol and precipitated with ethanol. The extracted RNAs were subjected to cDNA synthesis and reverse transcriptase with quantitative polymerase chain reaction (RT-qPCR).

The GST pull-down assay was performed similarly to the IP, except that Glutathione Sepharose 4 B Resin (GE Healthcare) was used instead of Protein G Agarose 4 B. As indicated, the cell extracts were treated with RNase A (MilliporeSigma) for 15 min at 37°C before incubation with either antibody-conjugated resin or glutathione-conjugated resin.

Protein expression, purification and the *in vitro* GST pull-down assay

Purification of the recombinant proteins and GST pull-down assays were performed as previously described (35,36,40). Briefly, *Escherichia coli* strain BL21(DE3)pLysS was transformed with a plasmid expressing GST, GST-eIF3g, GST-eIF4A3, His-eIF3g or His-eIF4A3. To induce the expression of the recombinant protein, 1 mM isopropyl-β-D-1-thiogalactopyranoside (IPTG) was added to the culture medium when the absorbance at 600 nm (A_{600}) reached 0.5. After incubation for 3 h at 37°C, the cells were harvested and lysed in lysis buffer [50 mM Tris-HCl (pH 8.0), 150 mM NaCl, 0.5% Triton X-100, 1 mM dithiothreitol, 10% (v/v) glycerol, 2 mM benzamidine hydrochloride and 1 mM PMSF].

For *in vitro* GST pull-down assays, glutathione Sepharose 4B with prebound GST-tagged recombinant proteins was mixed with a purified recombinant His-tagged recombinant protein in binding buffer [10 mM HEPES (pH 7.4), 1.5 mM magnesium acetate, 150 mM potassium acetate, 2.5 mM dithiothreitol and 0.05% Nonidet P-40] and incubated for 1 h at 4°C. After five washes with the binding buffer, the bound proteins were analyzed by western blotting.

Human and rabbit eIF3 were purified from HeLa cells and rabbit reticulocyte lysates (Green Hectares), respectively, following established procedures (49,50).

Western blotting

Primary antibodies against the following proteins were used for western blotting or IP: GST [catalog no. (#) A190-122A, Bethyl Laboratories], His tag (27–4710-01, GE Healthcare), HA tag (3F10; 11867431001, Roche), MYC tag (9E10; OP10L, Millipore), eIF4A3 [sc-365549, Santa Cruz Biotechnology; (51)], phospho-eIF4A3 (35), MLN51 (ab90651, Abcam), Y14 (MAB2484, Abnova), MAGOH (ab38768, Abcam), eIF1 (12496, Cell Signaling Technology), eIF3a (3411, Cell Signaling Technology), eIF3b (sc-16377, Santa Cruz Biotechnology or # A301-761A, Bethyl Laboratories), eIF3c (sc-28858, Santa Cruz Biotechnology), eIF3g (646101, BioLegend or # A301-757A, Bethyl Laboratories), eIF3i (11287–1-AP, Proteintech), eIF5 (11155–1-AP), 4E-BP1 (9452, Cell Signaling Technology), phospho-Ser^{65} 4E-BP1 (9451, Cell Signaling Technology), rpS3 (ab140688, Abcam), rpL11 (14382, Cell Signaling Technology), β-Catenin (9581, Cell Signaling Technology), β-actin (A5441, MilliporeSigma) and GAPDH (LF-PA0212, AbFrontier). In addition, horseradish peroxidase (HRP)-conjugated primary antibodies were used in our study [α-His-HRP (sc-8036 HRP, Santa Cruz Biotechnology) and α-FLAG-HRP (A8592, MilliporeSigma)].

The following secondary antibodies against the primary antibodies were used for western blotting: an HRP-conjugated goat anti-mouse IgG antibody (AP124P, MilliporeSigma), HRP-conjugated goat anti-rabbit IgG antibody (AP132P, MilliporeSigma), HRP-conjugated rabbit anti-goat IgG antibody (A5420, MilliporeSigma) and HRP-conjugated goat anti-rat IgG antibody (ab6845, Abcam).

Far western blotting

This procedure was performed as described previously (36,38). Briefly, purified rabbit and human eIF3 complexes were separated by SDS–polyacrylamide gel electrophoresis (PAGE) and transferred to a nitrocellulose membrane (GE Healthcare). Next, the membrane was incubated with purified recombinant His-eIF4A3 or bovine serum albumin (Bovogen), followed by conventional western blotting with the HRP-conjugated α-His antibody.

The *in situ* proximity ligation assay

The proximity ligation assay (PLA) was performed following the manufacturer's instructions. Briefly, HeLa cells grown on a coverslip were fixed with 3.8% formaldehyde in PBS (pH 7.4) for 30 min at room temperature, permeabilized with 0.5% Triton X-100 in PBS, incubated with blocking buffer for 1 h at 37°C and finally incubated with specific primary antibodies for additional 1 h at 37°C. After washing, the cells were incubated with the secondary antibodies conjugated with either PLUS or MINUS PLA probes [Duolink® In Situ PLA® Probe Anti-Mouse PLUS (MilliporeSigma; DUO92001) and Duolink® In Situ PLA® Probe Anti-Rabbit MINUS (MilliporeSigma; DUO92005), respectively] for 1 h at 37°C. The cells were subjected to ligation for 30 min at 37°C and rolling circle amplification using Duolink® In Situ

Detection Reagents Green (MilliporeSigma; DUO92014). 4′,6-Diamidino-2-phenylindole (DAPI) staining was performed to visualize the nucleus. Images were captured using an LSM800 microscope (Carl Zeiss).

Immunostaining

HeLa cells were fixed in 3.8% formaldehyde (MilliporeSigma) and permeabilized with 0.5% Triton X-100 (MilliporeSigma). Permeabilized cells were incubated for 1 h with 1.5% bovine serum albumin (BSA; BovoStar) for blocking, followed by incubation for 1 h with the primary antibody in PBS containing 0.5% BSA. Next, the cells were incubated in PBS containing 0.5% BSA with secondary antibodies conjugated to Alexa Fluor 488 or rhodamine (Life Technologies). DAPI was used to visualize the nuclei. Images were obtained using an LSM800 (Carl Zeiss).

The dual luciferase assay

FLuc and RLuc activities were measured using the Dual Luciferase Assay Kit (Promega) following the manufacturer's instructions. All raw data for the dual luciferase assay and RT-qPCR results obtained from each experiment are provided in Supplementary Table S3.

RT-qPCR

The isolation of total cell or cytoplasmic RNAs from cells and cDNA synthesis have been described previously (35,36,40). Total-cell or cytoplasmic RNAs were extracted using TRIzol Reagent (Thermo Fisher Scientific) following the manufacturer's instructions and were digested for 45 min at 37°C with 0.05 U/μl DNase I (Thermo Fisher Scientific) supplemented with 0.4 U/μl RiboLock RNase inhibitor. Where indicated, total-RNA samples were digested with 10 U/μl RNase R (Lucigen) for 15 min at 37°C. Purified RNAs were heated at 95°C for 5 min, followed by rapid chilling on ice for 5 min. Next, the denatured RNAs were subjected to cDNA synthesis in 20 μl reaction mixture at 37°C for 2 h with 6 U/μl RevertAid reverse transcriptase (Thermo Fisher Scientific) supplemented with an RNase inhibitor (1 U/μl) following the manufacturer's recommendations. After the reaction, the reverse transcriptase was inactivated by heating at 95°C for 5 min. RT-qPCR analysis was carried out with gene-specific oligonucleotides (Supplementary Table S1C) and LightCycler 480 SYBR Green I Master Mix (Roche) on a LightCycler 480 II machine (Roche). MIQE guidelines were followed to conduct the RT-qPCR experiments (52). Endogenous circRNAs were analyzed by RT-qPCR using divergent oligonucleotides previously validated as specific to circRNAs (36,53,54).

To prepare RNAs from the polysome-fractioned samples, polysomal and subpolysomal fractions were collected. Then, the total RNAs were extracted using equal volumes of phenol, chloroform and isoamyl alcohol. Subsequent RNA precipitation was performed with a single volume of isopropanol. The extracted RNAs were then treated with DNase I and reverse transcribed using the aforementioned methods.

RT-PCR analysis

Total-RNA samples (10 μg) were digested with 10 U/μl RNase R for 15 min at 37°C. After purification, the RNAs were subjected to cDNA synthesis. To detect circRNAs or linear RNAs, DNA fragments were amplified by PCR using cDNA as a template and a specific set of oligonucleotides (Supplementary Table S1C). Finally, the PCR products were resolved and analyzed using agarose gel electrophoresis.

Northern blotting

RNA probes for northern blotting were produced using *in vitro* transcription reactions involving T7 RNA polymerase and PCR-amplified DNA fragments as templates, in the presence of digoxigenin (DIG)-UTP (DIG RNA Labeling Kit; Roche). The oligonucleotides used for the amplification of the DNA template are listed in Supplementary Table S1D.

Total cell RNA was purified using the TRIzol Reagent. Electrophoresis of 15 μg of total RNA was carried out on a 1.2% denaturing agarose gel, and the RNA was transferred to a Hybond-N^+ membrane (Invitrogen). Next, the membrane was dried and crosslinked (0.12 J/cm^2) using a CL-1000 ultraviolet crosslinker (Ultra-Violet Products Ltd.). Prehybridization was performed at 68°C for 2 h, and hybridization was performed in Hybridization Buffer (Clontech) with a DIG-labeled RNA probe. The membrane was washed stringently (twice with 2 × SSC supplemented with 0.1% SDS and once with 0.5 × SSC supplemented with 0.1% SDS at 68°C), and the signals were developed using the DIG Luminescent Detection Kit (Roche).

In vitro transcription

SL-BoxB-R, BoxB-R and FLuc RNA were synthesized *in vitro* using linearized pcDNA3-SL-BoxB-R, pcDNA3-BoxB-R and pCI-FLuc, respectively, as templates, T7 RNA polymerase (New England Biolabs) and 2 mM of each NTPs. To obtain capped linear RNAs, an 8 mM cap analog (New England Biolabs) was added to the reaction mixture. To remove the DNA templates, DNase I was treated after *in vitro* transcription for 20 min at 37°C. DNase I-treated samples were then column-purified (New England Biolabs).

In vitro synthesis of circRNAs

In vitro circularization was performed as previously described (44). Briefly, to generate Circ-BoxB-R and Circ-R RNAs, linearized pSK-Circ-R and pSK-Circ-BoxB-R, respectively, were *in vitro*-transcribed. After *in vitro* transcription, the transcripts were treated with DNase I for 20 min at 37°C, followed by column purification (New England Biolabs). To increase circularization efficiency, the purified RNAs were recircularized as follows: the purified RNAs were heated at 70°C for 5 min, followed by rapid chilling on ice for 3 min. Next, 2 mM GTP was added to the reaction mixture with buffer [50 mM Tris-HCl (pH 7.5), 10 mM $MgCl_2$ and 1 mM DTT] to circularize the *in vitro*-synthesized RNAs. To remove the remaining linear RNAs, 20 μg of RNAs was heated at 65°C for 3 min and immediately cooled on ice for 3 min. Next, RNase R treatment was performed following the manufacturer's instructions. Finally, the RNase R-digested RNAs were purified on a column to obtain *in vitro*-circularized RNAs.

In vitro tethering-coupled translation

To prepare lysates of cells expressing an effector protein, HeLa cells were transiently transfected with a plasmid expressing λN-HA-GFP, λN-HA-eIF4A3-WT, λN-HA-eIF4A3 variant, λN-HA-Y14, λN-HA-MAGOH or λN-HA-MLN51. Two days later, the cell pellets were lysed using a hypotonic buffer

[10 mM Tris-HCl (pH 7.4), 10 mM NaCl, 0.1% (v/v) Triton X-100, 10 mM EDTA, 1 mM PMSF and 2 mM benzamidine hydrochloride], followed by incubation on ice for 30 min. After incubation, the cells were further disrupted with a narrow-gauge syringe. Next, 10 μl of cell lysates were mixed with 4 μl of *in vitro*-synthesized either linear or circular RNAs dissolved in DEPC-DW, 3 μl of TM [132 mM HEPES (pH 7.4), 112.2 mM creatine phosphate (MilliporeSigma), 0.66 μg/μl creatine phosphate kinase (Roche), 1 mM spermidine (MilliporeSigma), 264 μM amino acid (Promega), 6.6 mM rATP (New England Biolabs), 0.792 μM rGTP (New England Biolabs) and 13.2 mM DTT], 2 μl of HT buffer [10 mM HEPES (pH 7.4), 400 mM potassium acetate, 5 mM MgAc, 4 mM DTT and 10% glycerol], 0.4 μl of 2 mM potassium acetate, 0.4 μl of 25 mM magnesium acetate and 0.2 μl of 40 U/μl RNase inhibitor. The reaction mixtures were then incubated at 37°C for 1 h. Finally, the activities of *in vitro*-translated RLuc and FLuc were measured as described before.

The polysome fractionation experiment

Polysome fractionation of HeLa cell lysates (from three 150 mm culture dishes) was carried out as described previously (37,55). Briefly, the cells were preincubated with the normal growth medium supplemented with 100 μg/ml cycloheximide (MilliporeSigma) for 15 min to immobilize ribosomes on mRNAs. The cells were then washed once with PBS containing 100 μg/ml cycloheximide and resuspended in polysome cell extraction buffer [50 mM 3-(*N*-morpholino) propanesulfonic acid (pH 7.4), 15 mM $MgCl_2$, 150 mM NaCl, 100 μg/ml cycloheximide, 0.5% (v/v) Triton X-100, 1 mg/ml heparin (MilliporeSigma), 0.2 U/μl RiboLock RNase inhibitor, 2 mM PMSF and 1 mM benzamidine hydrochloride], followed by incubation for 10 min on ice. After centrifugation at 13 000 × *g* for 10 min, the supernatant (cytosolic fraction) was loaded onto a 10–50% (w/v) sucrose gradient bar and subjected to ultracentrifugation at 36 000 rpm for 2 h (Optima XE-90 Ultracentrifuge, Beckman Coulter) with the following settings: maximum speed and coarse break. Each fraction was collected using a Foxy Jr Density Gradient System (Teledyne ISCO) according to the A_{254}. Equal amounts of *in vitro*-synthesized FLuc RNA were added to each fraction as a spike-in control for normalization. For ribosome run-off experiments, the cells were treated with 100 μg/ml puromycin (Puro; MilliporeSigma) before harvesting.

CircRNA microarray analysis

For the transcriptome-wide identification of circRNAs that associate with polysomes in an eIF4A3-dependent manner, circRNA microarray analysis was performed using either polysomal or subpolysomal fractions from HeLa cells depleted or not depleted of eIF4A3, following Arraystar's standard protocols for the Human Circular RNA Array (8 × 15 K; AS-S-CR-H-V2.0, Arraystar). In brief, the RNAs were digested with RNase R (Epicenter) to remove linear RNAs. The remaining circRNAs were amplified and transcribed into fluorescent complementary RNAs using the random priming method (Arraystar Super RNA Labeling Kit; Arraystar). The labeled complementary RNAs were hybridized with the circRNA microarray. After the slides were washed, the arrays were scanned by an Agilent Scanner G2505C. The Agilent Feature Extraction software (v.11.0.1.1) was used to analyze the acquired array images.

Computational analysis was performed using the R language (v.3.6.1) with the Tidyverse (v.1.2.1) and Biostrings (v.2.52.0) packages powered by R Studio (v.1.1.456). The array signals with the quality status 'absent' or 'marginal' were removed from the data. The $\log_2$ values of normalized signal intensities ≥5.0 were arbitrarily selected. CircRNAs deposited in the circBase database (http://www.circbase.org/) were used for further analysis (4220 circRNAs). The relative ratios of the polysomal-to-subpolysomal levels of circRNAs (PS ratios) were calculated. To calculate the fold-change, the PS ratios of circRNAs in the cells depleted of eIF4A3 were divided by those of circRNAs in undepleted cells. To adjust the microarray data to the experimental data, a scaling factor (0.261 for set #1 and 0.262 for set #2) was applied to recalculate the fold-change. The scaling factor was experimentally determined by RT-qPCR analysis of cZNF609 and cGSE1 using the same pool of RNAs. For the analysis of the correlation between circRNA microarray data from two biological replicates, Pearson's correlation coefficients (*r*) were calculated. For statistical analysis, lmPerm (v.2.1.0) and DescTools (v.0.99.28) packages were used. CircRNA microarray data were deposited in the Gene Expression Omnibus database under the accession code GSE131563.

Statistical analysis

Two-tailed equal-variance Student's *t*-test was performed for statistical analysis with significance defined as a P value < 0.05 (high significance at $P < 0.01$). For transcriptome-wide analysis of circRNAs, the Wilcoxon signed-rank test or one-way ANOVA, followed by either Tukey's honestly significant difference test or Bonferroni correction, was performed to calculate statistical significance. In most cases, data from three biological replicates were analyzed unless otherwise specified in the figure legends. Data are presented as the mean ± standard deviation.

Results

eIF4A3 interacts with eIF3g, a component of the eIF3 complex

Initially, we screened for eIF4A3-interacting proteins using a yeast two-hybrid screening system with a GAL4 DNA-binding domain (BD)-fused human eIF4A3 as bait and a human thymus cDNA library fused with an activation domain (AD). From 3.5×10^7 colonies, we successfully isolated nine independent ones (Figure 1A): one for eIF3g (NM_003755), one for ZXDB (NM_007157) and seven colonies for NOM1 (NM_138400). Notably, a previous report showed that NOM1 interacts with eIF4A3 and participates in pre-rRNA processing (56).

Among the identified proteins, we selected eIF3g to investigate its specific interaction with eIF4A3. First, a yeast two-hybrid assay revealed that eIF3g specifically interacted with eIF4A3, but not with eIF4A1 and eIF4A2 (Supplementary Figure S1A), which are highly similar to eIF4A3 in amino acid sequence (57). In addition, eIF3g was the only eIF3 component that interacted with eIF4A3 (Figure 1B). Second, the direct interaction between eIF4A3 and eIF3g was evident from an *in vitro* GST pull-down assay based on recombinant eIF4A3 and eIF3g (Supplementary Figure S1B, C), far western blotting involving purified recombinant His-eIF4A3 and the eIF3 complex purified from rabbit or cultured human cells (Figure 1C),

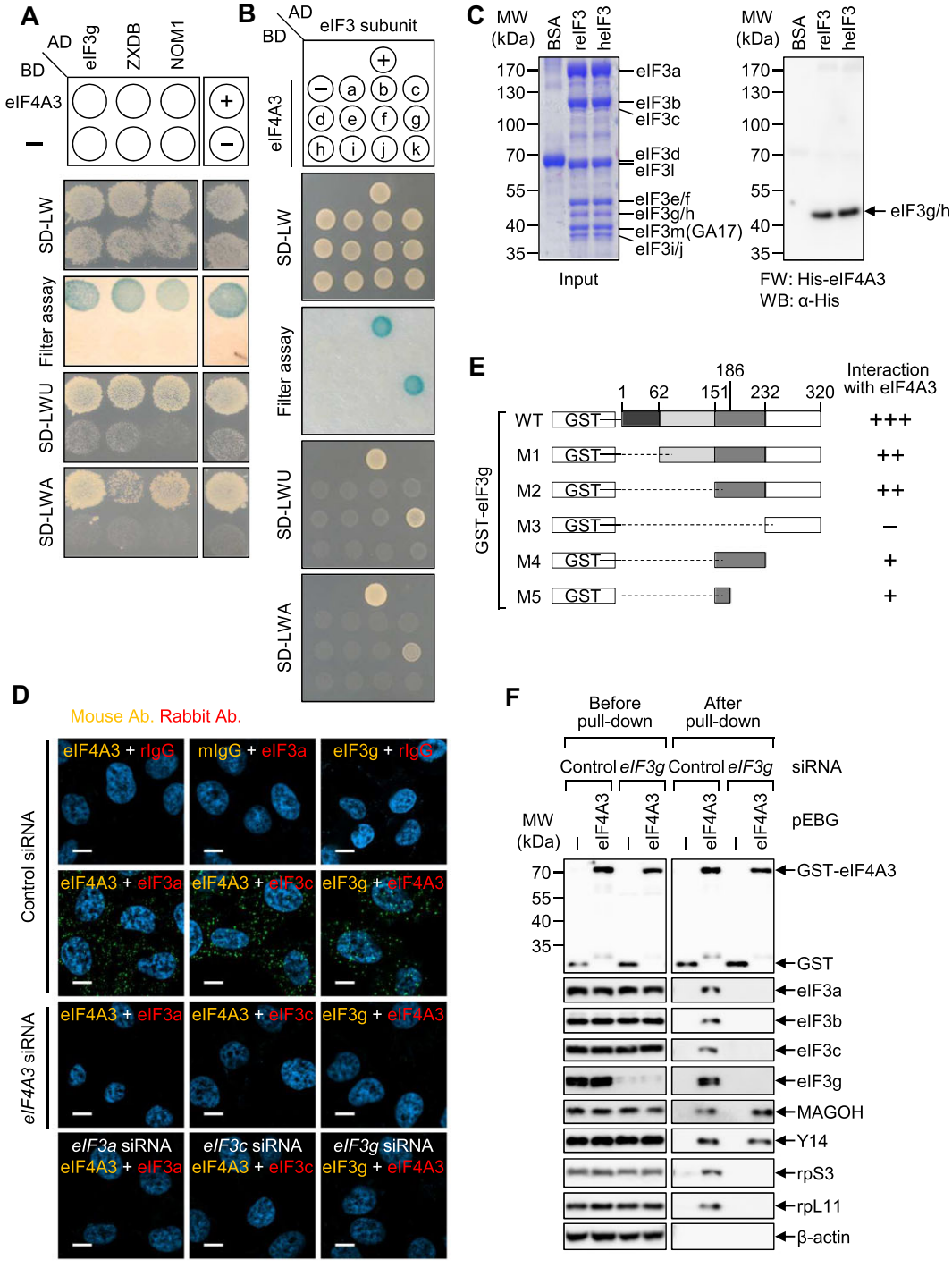

Figure 1. eIF4A3 interacts with eIF3g. (**A**) The yeast two-hybrid assay using BD-eIF4A3 and the indicated AD-fused preys. Transformed yeast cells were spread on a selective medium lacking leucine and tryptophan (SD-LW) to select cotransformants. In our system, specific interactions between BD-eIF4A3 and the AD-library were expected to yield a visible blue color (LacZ expression in the filter assay), and the growth on a medium lacking uracil (SD-LWU) and on a medium lacking adenine (SD-LWA). A known interaction, homodimerization of polypyrimidine tract-binding protein, served as the positive control (+). The empty vectors expressing BD or AD served as the negative control (–). (**B**) The yeast two-hybrid assay involving BD-eIF4A3 and AD-eIF3 subunits (all human proteins). (**C**) Far-western blotting analysis. Purified rabbit and human eIF3 complexes and bovine serum albumin (BSA, which served as a negative control) were resolved by SDS–PAGE. Next, the purified recombinant eIF4A3 and the α-His antibody were used as a probe and primary antibody, respectively. The representative images of Coomassie blue staining and a far-western blot are shown in the left and right panels, respectively. Because eIF3g and eIF3h comigrated in the SDS–PAGE gel under our conditions, we could not distinguish a specific interactor of eIF4A3. FW, far-western blotting; WB, western blotting. (**D**) The PLA assay to evaluate the interaction between EJC component and eIF3 components. HeLa cells either depleted or not depleted of the indicated protein were subjected to the PLA assay. The antibodies raised in a mouse or rabbit are colored yellow or red, respectively. mIgG, nonspecific mouse IgG; rIgG, nonspecific rabbit IgG; scale bar, 10 μm. (**E**) Mapping of the domains of eIF3g required for its interaction with eIF4A3. The results obtained from IP experiments with FLAG-eIF4A3 and either GST-eIF3g or its deletion variant (Supplementary Figure S2) are summarized. (**F**) The GST pull-down assay. HEK293T cells either undepleted or depleted of eIF3g were transiently transfected with a plasmid expressing either GST or GST-eIF4A3. Representative images from at least two biological replicates ($n = 2$) are presented in each panel.

IP experiments with endogenous eIF4A3 after RNase A treatment (Supplementary Figure S1D) and *in vivo* GST pull-down assay with GST-eIF3g (Supplementary Figure S1E). Third, we used a PLA, which provides a high level of specificity and enables the precise detection of protein–protein interactions within cells (58). Although our confocal microscopy analysis showed that the eIF4A3 and eIF3 components were mainly distributed in the nucleus and cytoplasm, respectively (Supplementary Figure S1F), the PLA results showed that the interaction of eIF4A3 with eIF3a, eIF3c and eIF3g occurred in both the nucleus and cytoplasm (Figure 1D). Moreover, the downregulation of either eIF4A3 or an eIF3 component by small interfering RNA (siRNA) almost completely inhibited PLA signals (Figure 1D). Finally, IP experiments with FLAG-eIF4A3 and either GST-eIF3g or its deletion variant revealed that the region corresponding to amino acid residues 151–186 of eIF3g was essential for binding to eIF4A3 (Figure 1E, Supplementary Figure S2). Collectively, these findings indicate a specific and direct interaction between eIF4A3 and eIF3g, both *in vitro* and *in vivo*.

An interaction of eIF4A3 with eIF3g links the EJC and eIF3 complex

Considering that eIF4A3 is a core component of the EJC (59,60) and that eIF3g is a component of a stable eIF3 subcomplex in mammals (5,8), it is plausible that the direct interaction of eIF4A3 with eIF3g may lead to the association of the EJC with the eIF3 complex. Indeed, our PLA assay revealed an *in vivo* interaction between either eIF4A3 or Y14 and the eIF3 component (Figure 1D, Supplementary Figure S1G). In addition, eIF3 components co-immunopurified with endogenous eIF4A3 (Supplementary Figure S1D) and vice versa (Supplementary Figure S1E). Notably, the association of eIF4A3 with eIF3 components and ribosomal proteins but not with other EJC components was almost completely disrupted when the cells were depleted of eIF3g (Figure 1F). These results indicate a specific association between the EJC and the eIF3 complex via the eIF4A3–eIF3g interaction.

A tethered eIF4A3 drives the internal initiation of translation

What is the molecular function of the eIF4A3 association with eIF3g? As the EJC is deposited onto mRNA after splicing, it may recruit eIF3 and ribosomes, thereby driving the internal initiation of translation of spliced mRNAs. Nonetheless, EJCs deposited onto newly synthesized linear mRNAs can be rapidly displaced from the mRNAs by translating ribosomes (61), making it difficult to experimentally determine the effect of eIF4A3 on internal initiation. Therefore, to more precisely determine the effect of EJC components on internal translation, we used intronless tethering reporter constructs containing (i) either a strong stem-loop (SL) structure ($\Delta G = -87.8$ kcal/mol) in the middle of the 5′UTR (SL-BoxB-R) or no such structure (BoxB-R), (ii) 12 repeats of the BoxB sequence derived from bacteriophage λ in the 5′UTR and (iii) a *Renilla* luciferase gene (RLuc; Figure 2A). An exogenously expressed λN-HA-tagged fusion protein was expected to be tethered to BoxB sequences located in the 5′UTR. In addition, consistent with previous findings showing that the presence of a strong SL structure in the 5′UTR blocks cap-dependent translation due to inefficient ribosome scanning (37,39), we observed that the insertion of an SL in the 5′UTR reduced RLuc activity by ∼10-fold (Supplementary Figure S3A). We also observed that tethering of a general translation initiation factor (eIF1, eIF3i or eIF5) to the 5′UTR of reporter SL-BoxB-R mRNA resulted in a ∼2-fold increase in relative RLuc activity (Supplementary Figure S3B, C), validating that our tethering system efficiently worked under the conditions used in our study.

Tethering of each EJC core protein (eIF4A3, Y14, MAGOH or MLN51) or eIF3g to the 5′UTR of reporter BoxB-R mRNA increased the relative RLuc activity by 2.1–4.0-fold without significantly influencing the abundance and integrity of the reporter mRNAs (see BoxB-R mRNA; Supplementary Figure S3D–F, left panels). A similar fold increase was also observed in the SL-containing reporter mRNA (see SL-BoxB-R mRNA; Supplementary Figure S3D–F, right panels). Notably, SL-BoxB-R mRNAs were significantly enriched in the IP of endogenous eIF4A3, when λN-HA-fused Y14, -MAGOH, -MLN51 or -eIF3g was co-expressed (Supplementary Figure S3G, H), suggesting that tethered Y14, MAGOH, MLN51 and eIF3g interact with endogenous eIF4A3 to a sufficient extent to drive the internal initiation of translation. Moreover, the observed increase in RLuc activity was significantly reversed when the EJC core component or the eIF3 component was downregulated (Figure 2B–D, Supplementary Figure S4A–C), suggesting that eIF4A3 drives internal initiation in an EJC- and eIF3-dependent manner.

Next, we conducted tethering experiments using various eIF4A3 variants: T163A, a non–phospho-mimetic form that stably associates with all other EJC core components (35); T163D, a phospho-mimetic form that cannot bind to all other EJC core components (35); D154K/Y155A and D401K/E402R, both of which fail to interact with MLN51 and a MAGOH-Y14 heterodimer, respectively (62); and E188Q, which lacks ATPase/helicase activity and loses the ability of eIF4A3 to interact with a heterodimer of MAGOH and Y14 (63). The results revealed that tethering eIF4A3-WT, T163A, T163D and E188Q led to a significant increase in relative RLuc activity compared to tethered GFP (Figure 2E). However, no such increase was observed for the D154K/Y155A or D401K/E402R mutations. Notably, T163A exhibited the highest increase in RLuc activity, and tethered T163D exhibited a weak but significant increase in RLuc activity compared with tethered GFP. Comparable expression of eIF4A3-WT and its variants was validated by western blotting (Supplementary Figure S4D). The specific interaction of eIF4A3 variants with other EJC components and eIF3g was also confirmed by IPs of the eIF4A3 variant (Figure 2F). Remarkably, eIF3g was preferentially enriched in the IPs of WT and T163A compared to the other eIF4A3 variants (Figure 2F). Collectively, these results indicate that eIF4A3 alone has an intrinsic ability to drive internal translation initiation in an eIF3-dependent manner and that this ability is enhanced by other EJC components.

The cellular EJC deposited onto mRNA after splicing drives the internal initiation of translation

To further elucidate eIF4A3-driven internal translation, we designed dicistronic constructs (Figure 3A), which contained—in the following order—the 5′UTR with or without a strong SL structure ($\Delta G = -87.8$ kcal/mol), a FLuc gene as the first cistron, an intercistronic region with or without the first intron of the β-globin gene (*Gl*) at 18 nucleotides downstream of a stop codon of the first cistron, and an RLuc gene as the

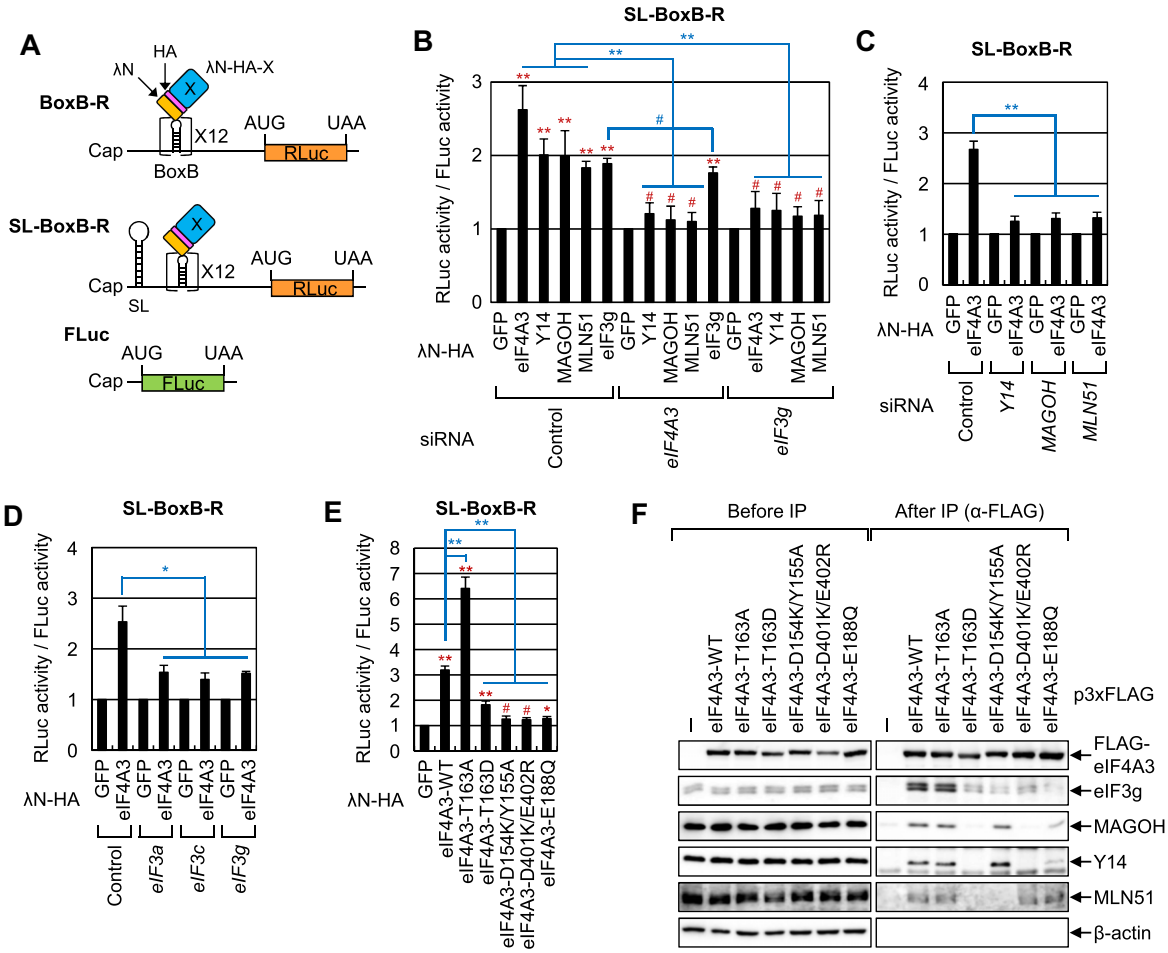

Figure 2. An eIF4A3 tethered to the 5′UTR drives the internal initiation of translation. (**A**) Schematic representation of tethering reporter mRNAs using 12 repeats of BoxB and λN system. AUG, a translation initiation codon; UAA, a translation stop codon; SL, a strong stem-loop structure; RLuc, *Renilla* luciferase; FLuc, firefly luciferase. (**B**) Artificial tethering of a core EJC component or eIF3g. HEK293T cells depleted of either eIF4A3 or eIF3g were cotransfected with a tethering reporter plasmid expressing SL-BoxB-R mRNA, an indicated effector plasmid and a reference plasmid (pGL3-control) expressing FLuc mRNA. Two days after transfection, cell extracts were subjected to dual luciferase assays. RLuc activities were normalized to FLuc activities. The normalized levels of RLuc activity in the presence of λN-HA-GFP were arbitrarily set to 1.0. Statistical significance between tethered λN-HA-GFP and other tethered proteins was calculated in each condition, and the corresponding *P* values are indicated by red asterisks. In addition, statistical significance among the depleted conditions was calculated, and the *P* values are indicated by blue asterisks with lines; $n = 4$; $^{**}P < 0.01$; #, not significant. (**C**) The effect of a tethered eIF4A3 on RLuc expression in cells depleted of one of EJC core components. As performed in (**B**), except that cells depleted of the indicated protein were transiently cotransfected with a plasmid expressing SL-BoxB-R mRNA, an indicated effector plasmid and pGL3-control; $n = 3$; $^{**}P < 0.01$. (**D**) The effect of tethered eIF4A3 on SL-BoxB-R mRNA in cells depleted of one of the eIF3 components; $n = 3$; $^{*}P < 0.05$. (**E**) The impact of the tethering of the eIF4A3-WT or its variant. HEK293T cells were transiently expressed with a plasmid expressing SL-BoxB-R mRNA, an effector plasmid expressing one of the eIF4A3 variants and pGL3-control. Statistical significance between tethered λN-HA-GFP and other tethered proteins was calculated, and the corresponding *P* values are indicated by red asterisks. In addition, statistical significance between tethered λN-HA-eIF4A3-WT and its variant was calculated, and the *P* values are indicated by blue asterisks with lines; $n = 3$; $^{**}P < 0.01$; $^{*}P < 0.01$; #, not significant. (**F**) Specific interaction of eIF4A3 variants with other EJC core components and eIF3g. Total-cell extracts of HEK293T cells transiently expressing FLAG-eIF4A3-WT or its variant were subjected to IP experiments using α-FLAG antibody. Co-immunopurified proteins were analyzed by western blotting. Representative images ($n = 2$) are presented in the panel.

second cistron. The Gl1 and Gl3 reporter mRNAs are expected to carry no EJCs and a single EJC, respectively, although they could produce mRNAs with identical nucleotide sequences. The same was true for Gl2 and Gl4 mRNAs. In addition, given that the EJC is deposited 20–24 nucleotides upstream of an exon–exon junction (64), Gl3 and Gl4 mRNAs are expected to carry an EJC upstream of the stop codon of the first cistron. However, an elongating ribosome in the first cistron would displace the EJC on Gl3 mRNAs. In the case of Gl4 mRNA, the EJC should remain on the mRNAs because the insertion of a strong SL structure into the 5′UTR is known to drastically inhibit cap-dependent translation by blocking ribosome scanning (37,39). Indeed, Gl4 mRNAs were found to be enriched preferentially over other reporter mRNAs in the IP of endogenous eIF4A3 (Figure 3B, Supplementary Figure S5A).

We assessed the effect of SL on the translational efficiency (luciferase activity normalized to the mRNA level) of FLuc and RLuc cistrons. SL insertion strongly blocked FLuc expression in both intronless and intron-containing mRNAs (Figure 3C; compare FLuc values between Gl1 and Gl2, and between Gl3 and Gl4), indicating a strong inhibitory function of SL. By contrast, RLuc cistron translation in intronless mRNAs was almost basal and was only marginally affected by SL

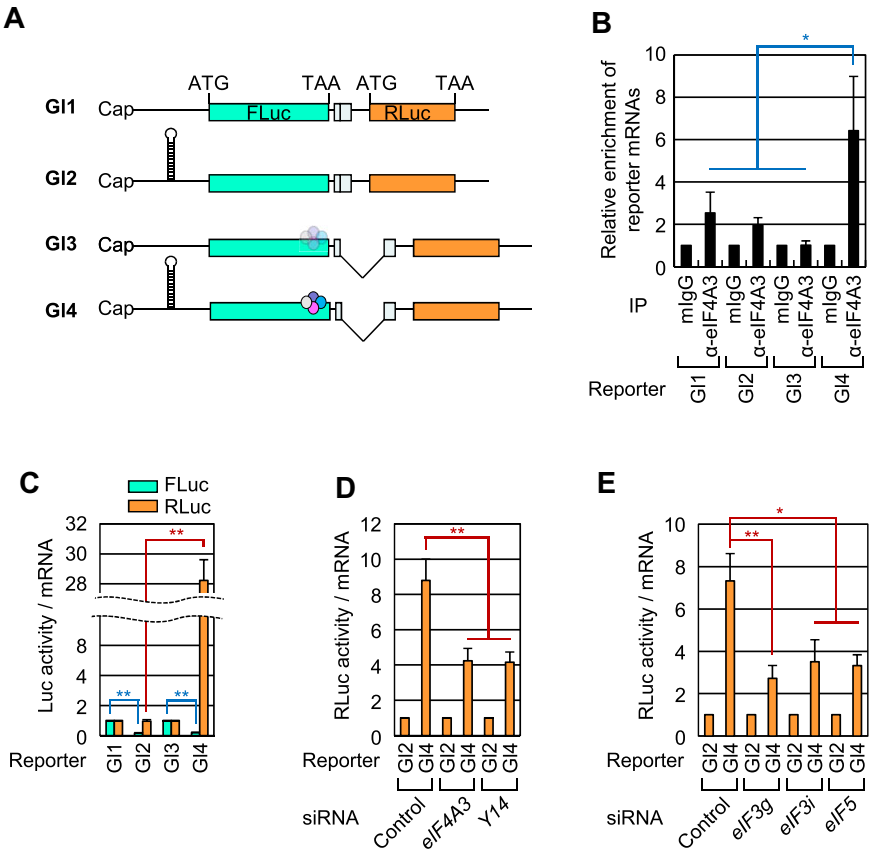

Figure 3. An endogenous EJC loaded onto mRNA after splicing drives the internal initiation of translation. (**A**) Schematic representation of dicistronic reporter mRNAs either containing or not containing the first intron of the β-globin gene in the intercistronic region. The EJCs deposited after splicing are depicted on the mRNAs. The EJCs that will be displaced by a translating ribosome are semitransparent. (**B**) RNA-IP of endogenous eIF4A3. Extracts of HEK293T cells transiently expressing one of the dicistronic reporter mRNAs were subjected to IP using the α-eIF4A3 antibody or, as a negative control, mouse (m) IgG. The levels of co-IPed reporter mRNAs were normalized to those of intronless *HIST2H2AA3* mRNA. The normalized levels of reporter mRNAs obtained in the IPs with mIgG were arbitrarily set to 1.0; $n = 4$; $^{*}P < 0.05$. (**C**) Translation efficiency of dicistronic reporter mRNAs. HEK293T cells were transfected with one of the dicistronic reporter plasmids. Next, the activities of proteins RLuc and FLuc and levels of reporter mRNAs were analyzed. FLuc and RLuc activities obtained from Gl1 and Gl3 were arbitrarily set to 1.0, respectively; $n = 3$; $^{**}P < 0.01$. (**D**) The effect of downregulation of an EJC component on dicistronic reporter mRNAs. As performed in (**C**), except that the cells were depleted of either eIF4A3 or Y14. The RLuc activities of Gl2 mRNA were arbitrarily set to 1.0, respectively; $n = 3$; $^{**}P < 0.01$. (**E**) The effect of downregulation of eIF3g, eIF3i, or eIF5 on dicistronic reporter mRNAs. As performed in (**D**), except that the cells were depleted of the indicated protein; $n = 3$; $^{**}P < 0.01$; $^{*}P < 0.05$.

insertion (Figure 3C, compares RLuc values between Gl1 and Gl2). Notably, in the case of the intron-containing mRNAs, its RLuc expression was significantly increased by SL insertion (Figure 3C, compares RLuc values between Gl3 and Gl4). Comparable expression and integrity of the reporter mRNAs were validated by northern blotting (Supplementary Figure S5B). To assess eIF4A3-dependent internal translation more specifically, we compared the RLuc expression levels between Gl2 and Gl4. The results showed that the downregulation of eIF4A3, Y14, eIF3g, eIF3i or eIF5 reversed the observed increase without affecting mRNA levels or integrity (Figure 3D, E, Supplementary Figure S5C–F). Considering that the EJC preferentially remains on Gl4 mRNA due to SL (Figure 3B), these findings indicate that cellular EJCs deposited onto mRNAs after splicing can drive the internal initiation of translation.

In vitro-synthesized linear mRNAs and circRNAs are translated in an eIF4A3-dependent manner

To corroborate eIF4A3-driven internal initiation, we performed an *in vitro* translation assay using *in vitro*-synthesized BoxB-R or SL-BoxB-R mRNAs (either capped or uncapped) and cytoplasmic extracts of HeLa cells expressing λN-HA-GFP, λN-HA-eIF4A3-WT or λN-HA-eIF4A3-T163D. As expected, the presence of SL decreased RLuc expression by ∼3.5–4.0-fold under our conditions, regardless of the 5′-cap (Figure 4A). Notably, a tethering of eIF4A3-WT to *in vitro*-synthesized SL-BoxB-R mRNAs promoted relative RLuc expression more strongly than a tethering of eIF4A3-T163D, regardless of the presence of the 5′-cap structure (Figure 4B). Therefore, our *in vitro* analyses using linear reporter mRNAs provide strong evidence for the eIF4A3-driven internal initiation of translation.

Recent advances in RNA sequencing have enabled the identification of numerous endogenous circRNAs (11,12,65). Notably, some circRNAs have been shown to be translated (14–17,19–24,28). Because circRNAs lack a 5′-cap structure (11,12), internal initiation of translation is the only way to synthesize proteins. To clearly demonstrate eIF4A3-driven internal translation, we used circRNA reporter plasmids to express circRNAs within cells. A limitation of this approach is that circRNA-expressing constructs can also generate linear mRNAs originating from *trans*-splicing by-products in the

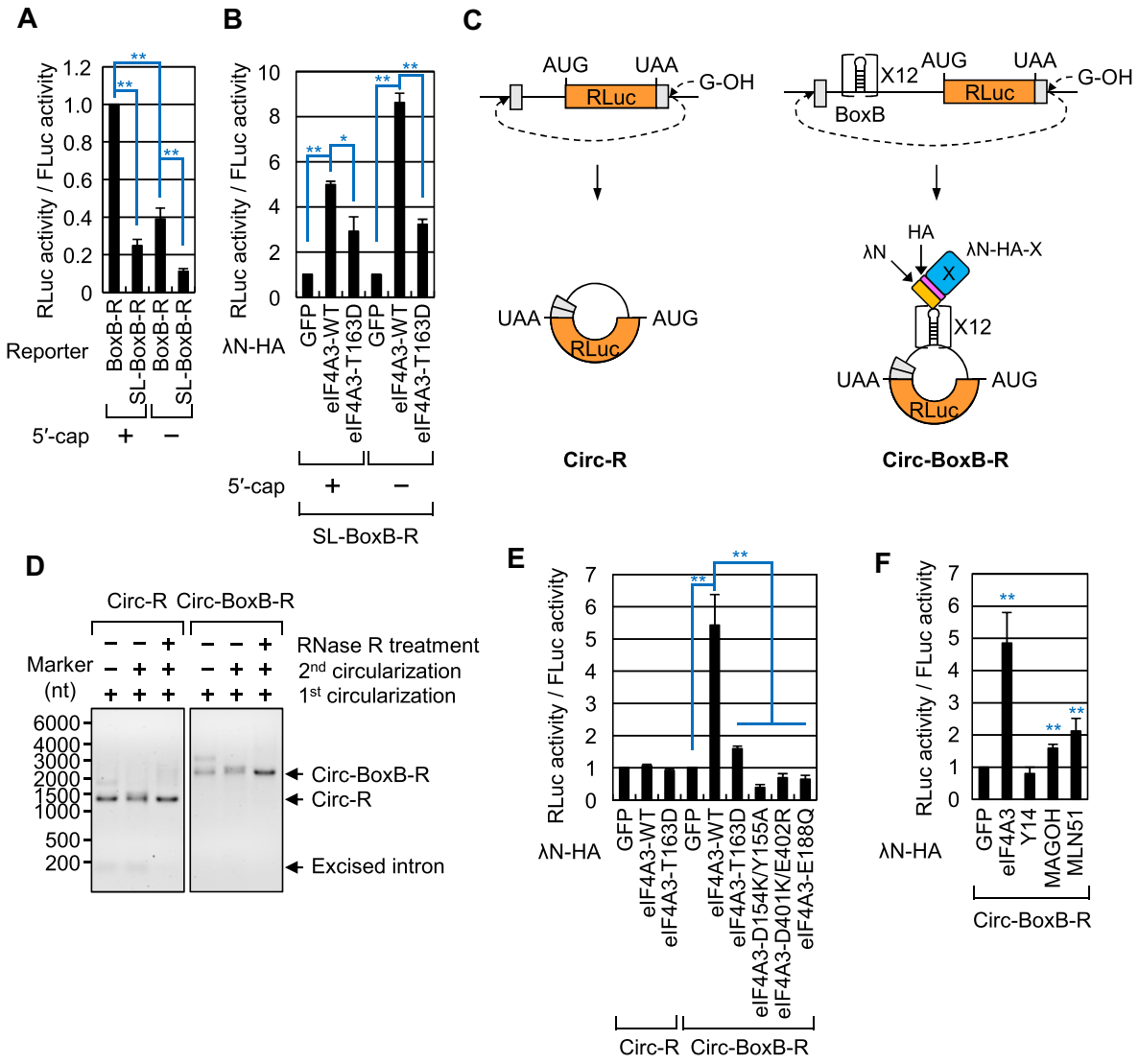

Figure 4. An eIF4A3 drives internal translation in the *in vitro* system. (**A**) The effect of an SL on *in vitro* translation. *In vitro*-synthesized BoxB-R or SL-BoxB-R RNA (either capped or uncapped) and *in vitro*-synthesized capped FLuc RNA were mixed with the cytoplasmic extracts of HeLa cells. RLuc activities were normalized to FLuc activities. The normalized levels of RLuc activity obtained from BoxB-R RNA were arbitrarily set to 1; $n = 3$; $^{**}P < 0.01$. (**B**) The *in vitro* translation assay using *in vitro*-synthesized linear reporter RNAs. *In vitro*-synthesized reporter RNA (SL-BoxB-R mRNA, either capped or uncapped) and *in vitro*-synthesized capped FLuc RNA were mixed with the cytoplasmic extracts of HeLa cells expressing the indicated effector protein. RLuc activity was normalized to FLuc activity. The normalized levels of RLuc activity in the extracts of the cells expressing λN-HA-GFP were arbitrarily set to 1; $n = 3$; $^{*}P < 0.05$; $^{**}P < 0.01$. (**C**) A schematic diagram of *in vitro* transcription followed by *in vitro* circularization. (**D**) Validation of *in vitro*-synthesized circRNAs by denaturing agarose gel electrophoresis. To maximize the yield of circRNAs, we carried out the circularization reaction twice. The details are described in the Methods section. (**E**) The *in vitro* translation assay using *in vitro*-synthesized circRNAs. As performed in panels (**A**) and (**B**), except that *in vitro*-synthesized circRNAs were mixed with the cytoplasmic extracts of HeLa cells expressing the indicated effector protein; $n = 3$; $^{**}P < 0.01$. (**F**) The effect of the tethered EJC on the translation of *in vitro*-synthesized circRNAs. As performed in (**E**), except that *in vitro*-synthesized Circ-BoxB-R RNAs were mixed with the cytoplasmic extracts of HeLa cells expressing the indicated effector protein; $n = 6$; $^{**}P < 0.01$.

cell (66). Therefore, to overcome this limitation, we utilized *in vitro*-synthesized circRNA reporters containing the RLuc gene and either harboring (Circ-BoxB-R) or not (Circ-R) harboring BoxB sequences (Figure 4C, D; ref. 44). The *in vitro*-synthesized linear FLuc mRNA (which served as a control for *in vitro* translation reactions) and either Circ-BoxB-R or Circ-R RNA were mixed with the cytoplasmic extracts of HeLa cells expressing λN-HA-GFP, λN-HA-eIF4A3-WT or a variant of eIF4A3. In agreement with our cell-based assay data with linear reporter mRNAs (Figures 2 and 3), a tethering of eIF4A3-WT to Circ-BoxB-R, but not to Circ-R, caused a significant increase in RLuc activity (Figure 4E). By contrast, other tested eIF4A3 mutants (T163D, D154K/Y155A, D401K/E402R and E188Q) only marginally or weakly increased the activity of RLuc expressed from Circ-BoxB-R (Figure 4E). Notably, T163D caused a weak but significant increase in RLuc from Circ-BoxB-R compared to GFP, suggesting that eIF4A3 itself has the ability to drive the internal initiation of translation. Furthermore, a tethering of another EJC component (MAGOH or MLN51) to Circ-BoxB-R yielded a significant increase in RLuc activity (Figure 4F). In the case of Y14, the expression of λN-HA-Y14 caused an increase in both RLuc and FLuc activities, in line with previous observations that Y14 is engaged in general cap-dependent translation

(67,68). Because of this property, we were unable to observe an increase in RLuc activity when Y14 was tethered to Circ-BoxB-R. Notably, the relative levels of Circ-R or Circ-BoxB-R did not change significantly after *in vitro* translation reactions under our conditions (Supplementary Figure S6). Considering the results obtained from the linear reporter mRNAs (Figures 2–4), these findings strongly suggest that eIF4A3 possesses an inherent capacity to initiate translation internally and this ability is further enhanced by the presence of other EJC components.

eIF4A3 promotes polysomal distribution of endogenous circRNAs

Next, we investigated whether eIF4A3 influences the translatability of endogenous circRNAs. To this end, we first tested three endogenous circRNAs, all of which were identified by high-throughput sequencing of polysome-bound circRNAs and experimentally validated as polysome-associated circRNAs (16): cFANCA (consisting of two exons; 203 nts in total length), cGSE (one exon; 219 nts) and cKANSL1 (two exons; 12261 nts). In addition, previously characterized translatable cZNF609 (1 exon; 874 nts; (14) and subpolysome-enriched cARL67P1 (2–6 exons; 254–2264 nts; (16) were analyzed in parallel as positive and negative control circRNAs, respectively, for polysome association.

First, in line with previous reports (14,16), a significant proportion of all tested endogenous circRNAs, except cARL67P1, were present in the polysomal fractions (∼24–38% of the total; Figure 5A, B). The observed polysomal distribution was significantly reduced by treatment with puromycin (Puro), a potent translation inhibitor. Moreover, linear *GAPDH* mRNAs, known to harbor approximately eight EJCs and be efficiently translated in a cap-dependent manner, were strongly associated with polysomes and their distribution significantly shifted from polysomes to subpolysomes upon Puro treatment. Second, the downregulation of either eIF4A3 or Y14 caused a significant redistribution of polysome-associated circRNAs from the polysomal to the subpolysomal fractions (Figure 5C–E, Supplementary Figure S7A, B). The observed redistribution caused by eIF4A3 downregulation was reversed by complementation with exogenous eIF4A3-WT (Figure 5C–E). By contrast, the relative distributions of cARL67P1 and endogenous linear mRNA (*GAPDH* mRNA) were not significantly affected by the downregulation of the EJC component. Finally, the efficient association of the tested endogenous circRNAs (except cARL67P1) with EJC or eIF3g was validated by RNA-IPs of an EJC component or eIF3g (Supplementary Figure S7C–J). In the case of endogenous cARL67P1, it was significantly enriched in the IP of an EJC component but not eIF3g. Considering a report suggesting that cARL67P1 is not efficiently enriched in polysomes (16), the inefficient polysomal association of cARL67P1 may be due to the weak interaction of cARL67P1 with eIF3g for an unknown reason. Collectively, these findings indicate that the polysomal association of endogenous circRNAs depends on eIF4A3 deposited onto circRNAs after back-splicing.

The eIF4A3-driven internal initiation of translation is resistant to cellular stresses

Various cellular stresses such as serum starvation cause an inhibition of 5′-cap-dependent translation via inefficient phosphorylation of eIF4E-binding protein 1 (4E-BP1) (1,2). We next investigated the effects of cellular stress on eIF4A3-driven internal initiation.

Serum starvation of cells for one day resulted in a reduction in the level of phosphorylated 4E-BP1 (Figure 6A), a decrease in the overall polysome peak (Figure 6B) and a redistribution of endogenous *GAPDH* mRNA from the polysomal to subpolysomal fractions (Figure 6C), validating the inefficient cap-dependent translation under these conditions. Importantly, the distribution of polysome-associated circRNAs did not change significantly in response to serum depletion (Figure 6C), suggesting that the internal translation of circRNAs is relatively resistant to cellular stress compared to the general cap-dependent translation. Supporting this conclusion, we also observed that tethered eIF4A3 increased RLuc activity expressed from the SL-BoxB-R reporter mRNA and this increase was not affected by serum starvation (Figure 6D, E) or overexpression of 4E-BP1 (Figure 6F, G). By contrast, FLuc activity, expressed by cap-dependent translation, was significantly reduced on serum depletion or 4E-BP1 overexpression. Collectively, our results support the notion that eIF4A3 drives internal translation even when general cap-dependent translation is compromised under stressful conditions.

Polysomal association of endogenous circRNAs depends on eIF4A3 at the transcriptome level

Based on the observations mentioned previously, we performed circRNA microarray analysis using a pool of polysome- or subpolysome-associated circRNAs obtained from cells depleted or not depleted of eIF4A3 for a transcriptome-wide analysis of circRNA translation (Figure 7A). We selected a circRNA microarray for this purpose because of its higher efficiency in circRNA profiling compared to RNA-seq (69). Additionally, we found that the circRNA microarray produced more reliable results than RNA-seq. The Pearson correlation coefficient (r) between two independent circRNA microarray experiments (two biological replicates, sets #1 and #2) was >0.900, indicating a strong correlation between the two replicates (Supplementary Table S4A). For subsequent analysis, endogenous circRNAs that were not enriched in the subpolysomal or polysomal fractions were excluded. In addition, endogenous circRNAs with low or basal expression levels were excluded to ensure higher stringency. The circRNA microarray results were then validated using RT-qPCR (Supplementary Figure S8A–C).

Analysis of the circRNAs from the overlap between the two sets revealed that the polysomal association of circRNAs decreased when eIF4A3 was downregulated (Figure 7B, Supplementary Table S4B). Moreover, circRNAs with higher enrichment in polysomes manifested a greater reduction in polysome association after eIF4A3 downregulation (Figure 7C). By contrast, the polysomal distribution of circRNAs and eIF4A3 dependence of the polysomal association of circRNAs were not significantly influenced by the length (Figure 7D, E) or type (Figure 7F, G) of circRNAs, the number of exons in circRNAs (Figure 7H, I) or the relative position of a putative translation stop codon and back-splicing junction (BSJ) within circRNAs (Supplementary Figure S8D, E). Collectively, these findings indicate that the efficient polysomal association of endogenous circRNAs requires eIF4A3.

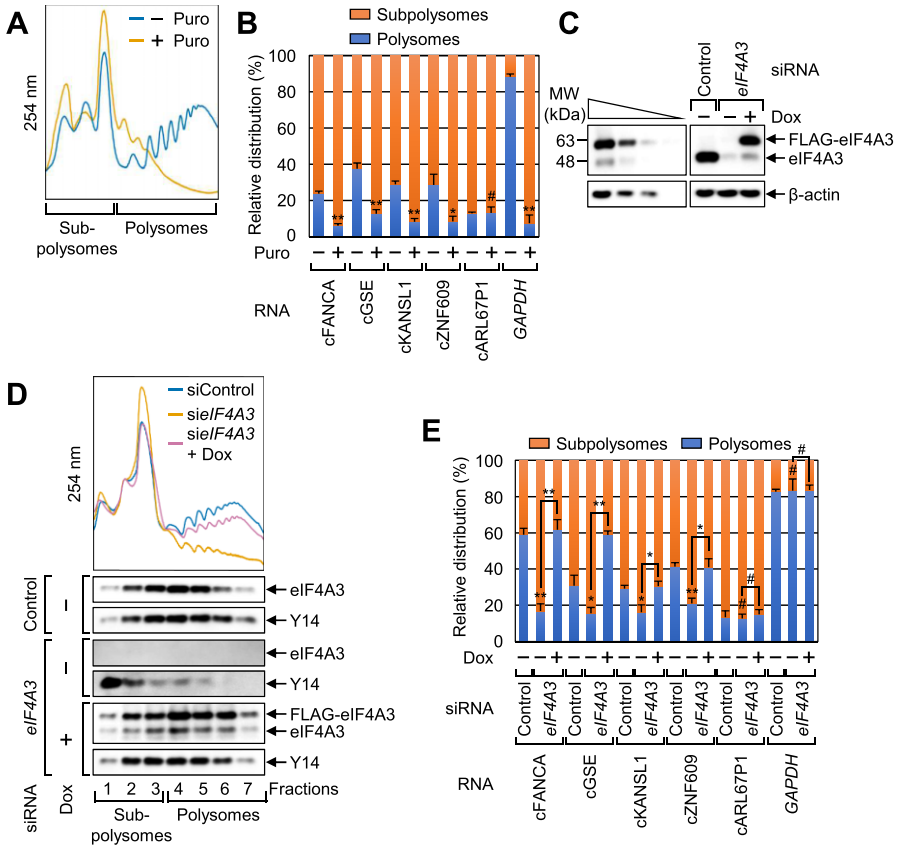

Figure 5. Polysomal association of endogenous circRNAs depends on the eIF4A3 and is resistant to serum depletion. **(A, B)** The effect of Puro treatment on relative polysomal distributions of endogenous circRNAs. Subpolysomal fractions (containing subunits the 40S, 60S and 80S) and polysome fractions of HeLa cells either treated or not treated with Puro for 2 h were pooled. Next, *in vitro*-synthesized FLuc RNA, as a spike-in control, was added to the pooled fractions. (**A**) Polysome profiles of cytoplasmic extracts of HeLa cells either treated or not treated with Puro. (**B**) Quantitative representation of endogenous circRNAs in subpolysomal and polysomal fractions. The endogenous circRNAs in the subpolysomal and polysomal fractions were quantitated by RT-qPCRs using circRNA-specific divergent oligonucleotides; $n = 3$; $^{**}P < 0.01$; $^{*}P < 0.05$; #, not significant. (**C–E**) The change in relative polysomal distributions of endogenous circRNAs after downregulation of eIF4A3 and complementation with siRNA-resistant FLAG-eIF4A3. (**C**) Western blotting validating specific downregulation of endogenous eIF4A3 and induction of FLAG-eIF4A3 up to a level comparable to that of endogenous eIF4A3. (**D**) Polysome profiles (upper) and relative distributions of endogenous proteins (lower). (**E**) Relative polysomal distributions of endogenous circRNAs. After polysome fractionation, *in vitro*-synthesized FLuc RNA, as a spike-in control, was added to the subpolysomal and polysomal fractions. The endogenous circRNAs in the subpolysomal and polysomal fractions were quantitated by RT-qPCRs using divergent oligonucleotides. Next, the levels were normalized to those of FLuc RNA. Relative distributions of endogenous circRNAs in the subpolysomal and polysomal fractions are presented as percentages; $n = 3$; $^{*}P < 0.05$; $^{**}P < 0.01$; #, not significant.

eIF4A3-driven internal translation of endogenous circRNA can generate a full-length intact protein

Our transcriptome-wide analysis revealed that 142 out of the 5901 endogenous circRNAs contained exons encoding a full-length protein that was identical to the protein generated from the linear mRNA (Figure 7, Supplementary Table S4B). Among the 142 circRNAs, we selected and functionally characterized circCTNNB1 (cCTNNB1) generated from the *CTNNB1* gene encoding β-catenin, a key protein in Wnt/β-catenin signaling (Figure 8A, B) (70). In our analysis, three isoforms of cCTNNB1 (which we termed cCTNNB1a, cCTNNB1b and cCTNNB1c) were detectable in all the tested human cell lines at different ratios (Supplementary Figure S9A, B). One report showed that cCTNNB1b expresses a truncated form of β-catenin protein and affects liver cancer cell growth (71). Among the three isoforms, only cCTNNB1c was expected to contain exons encoding full-length β-catenin (Figure 8A, B).

Using TOPFlash and FOPFlash reporter systems (43), we investigated whether endogenous cCTNNB1c RNA generates functionally active full-length β-catenin. TOPFlash and FOPFlash contained the *FLuc* gene under the control of a thymidine kinase minimal promoter with wild-type and mutated versions of T-cell factor (TCF)-binding sites, respectively (Figure 8C). It is well known that β-catenin protein induction caused by Wnt3a treatment activates TCF-dependent transcription (43).

Under our conditions, treatment with Wnt3a specifically increased the amount of β-catenin and induced FLuc expression from TOPFlash, but not from FOPFlash (Figure 8D, E). Remarkably, the observed induction was significantly inhibited by specific downregulation of either endogenous cCTNNB1c RNA or endogenous linear β-catenin mRNA (Figure 8E). Furthermore, the inhibition observed with siRNAs against endogenous linear β-catenin mRNA and endogenous cCTNNB1c RNA was almost completely and partially reversed, respectively, by transfection with pFLAG-cCTNNB1c expressing a circRNA encoding FLAG-cCTNNB1c (Figure 8F, Supplementary Figure S9C–E). It should be noted that under our conditions, exogenously

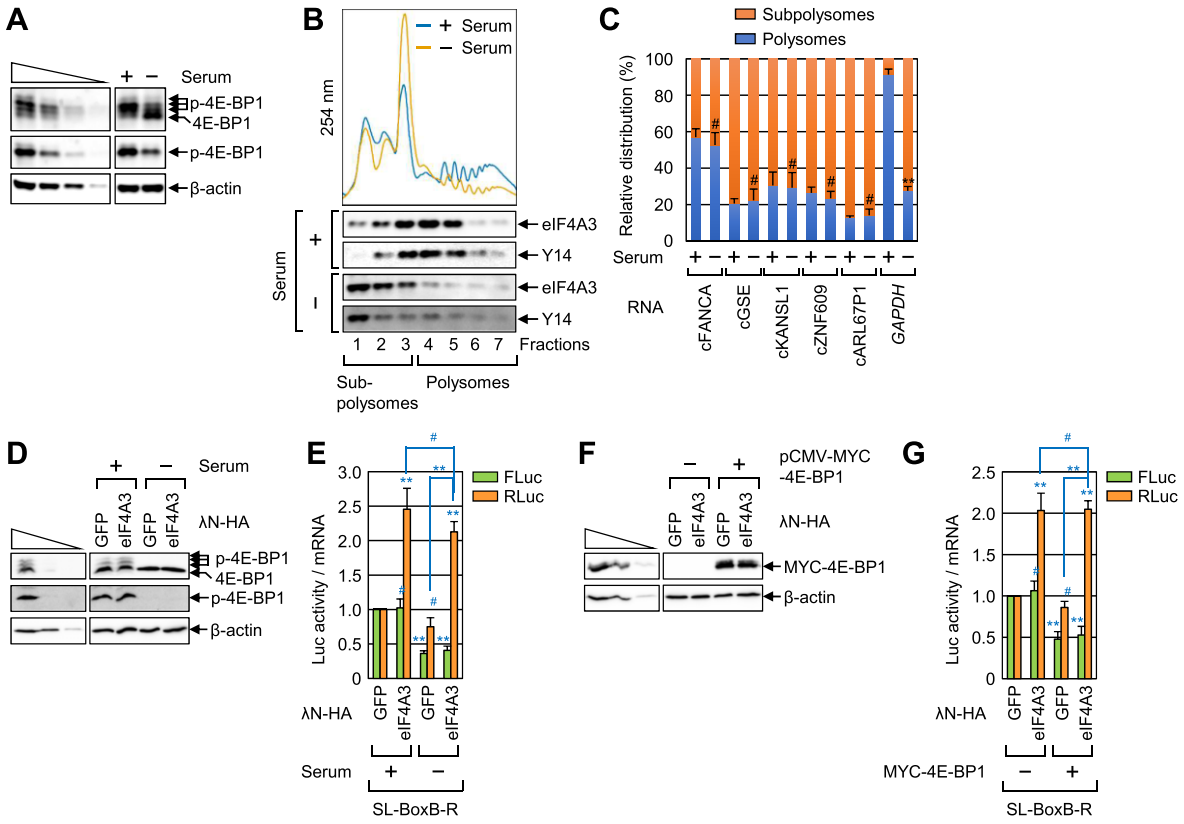

Figure 6. Internal initiation of translation driven by eIF4A3 is resistant to cellular stresses. (**A–C**) Lack of significant change in relative polysomal distributions of endogenous circRNAs after serum depletion. As performed in Figure 5A, B, except that HeLa cells were incubated in either a serum-containing or serum-free medium for 24 h before cell harvesting. (**A**) Western blotting showing 4E-BP1 dephosphorylation induced by serum depletion. (**B**) Polysome profiles (upper) and the relative distributions of endogenous proteins (lower). (**C**) Relative polysomal distributions of endogenous circRNAs; $n = 3$; $^{**}P < 0.01$; #, not significant. **(D, E)** The relative resistance of eIF4A3-mediated internal translation of linear mRNAs in response to serum depletion. HEK293T cells transiently expressing SL-BoxB-R mRNA, FLuc mRNA and either λN-HA-GFP or λN-HA-eIF4A3 were incubated in either a serum-containing or serum-free medium for 24 h before cell harvesting. (**D**) Western blots showing inefficient phosphorylation of 4E-BP1 on serum depletion. (**E**) Dual luciferase assay. RLuc and FLuc activities were normalized to total protein amounts. The normalized levels of RLuc and FLuc activities obtained from the cells expressing λN-HA-GFP in the serum-containing media were arbitrarily set to 1.0; $n = 3$; $^{**}P < 0.01$; #, not significant. **(F, G)** The relative resistance of eIF4A3-mediated internal translation of linear mRNAs in response to 4E-BP1 overexpression. HeLa cells were transiently expressed with SL-BoxB-R mRNA, FLuc mRNA, either λN-HA-GFP or λN-HA-eIF4A3, and either MYC or MYC-4E-BP1. (**F**) Western blots showing overexpressed MYC-4E-BP1. (**G**) Dual luciferase assay. RLuc and FLuc activities were normalized to total protein amounts. The normalized levels of RLuc and FLuc activities obtained from the cells expressing λN-HA-GFP and MYC were arbitrarily set to 1.0; $n = 3$; $^{**}P < 0.01$; #, not significant.

expressed FLAG-cCTNNB1c and endogenous cTNNB1c were targeted for rapid degradation by siRNA against cCTNNB1c RNA. Because of this property, it is likely that transfection with pFLAG-cCTNNB1c may cause a partial restoration of Wnt3a-induced FLuc expression (Figure 8F). In addition, the complementary sequences in flanking introns within the plasmid pFLAG-cCTNNB1c are known to trigger back-splicing (42), generating the circRNA encoding FLAG-cCTNNB1c (Supplementary Figure S9C–E). As a consequence of back-splicing, the generated circRNA was expected to have an EJC and express FLAG-cCTNNB1c via eIF4A3-dependent internal initiation, which was confirmed under our conditions (Supplementary Figure S9C–E). Therefore, our results from the complementation experiments suggest that although circRNAs are weakly translated compared with linear mRNA, the level of β-catenin protein above a threshold could be achieved by β-catenin protein expression from either circRNAs or linear β-catenin mRNA, regardless of the relative amounts of cCTNNB1 RNA or linear β-catenin mRNA. In addition, several studies have shown that for efficient activation of the Wnt/β-catenin pathway, the β-catenin protein level should reach a value above a specific threshold through either a positive or negative feedback loop (72–75).

We also observed that the polysomal distribution of endogenous cCTNNB1c RNA, but not that of its corresponding linear β-catenin mRNA, was significantly inhibited when the cells were depleted of eIF4A3 (Figure 8G) or eIF3g (Figure 8H). Taken together, these findings indicate that endogenous cCTNNB1c RNA can express functionally active full-length β-catenin in an eIF4A3-dependent manner.

Discussion

In this study, we provide molecular evidence for the active role of eIF4A3 in ribosome recruitment for the internal initiation of translation. Based on our work here and previous findings (76), we propose a model for the eIF4A3-driven internal translation of circRNAs as follows (Figure 9A): eIF4A3 (as a component of the EJC) deposited onto circRNAs generated by back-splicing recruits the eIF3 complex via a direct interaction between eIF4A3 and eIF3g (in this study). The other EJC core components help stabilize the eIF4A3-eIF3 interaction,

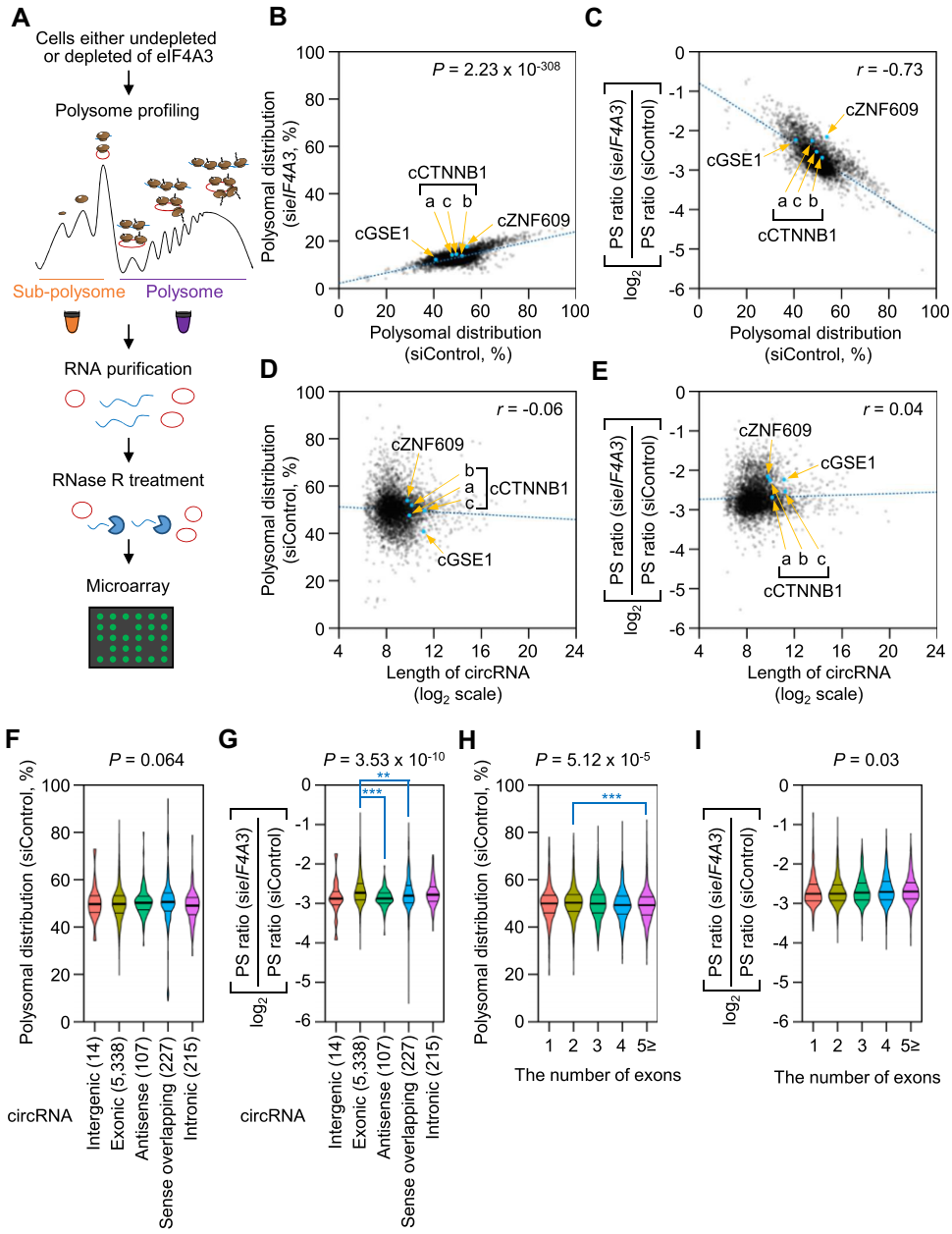

Figure 7. Polysomal enrichment of endogenous circRNAs is dependent on eIF4A3 at the transcriptome level. (**A**) The experimental scheme of polysome fractionation procedures followed by circRNA microarray. Cytoplasmic extracts of HeLa cells, either depleted or not depleted of eIF4A3, were subjected to polysome fractionation. Next, RNA samples purified from either the pooled subpolysomal or polysomal fractions were subjected to the circRNA microarray analysis; $n = 2$. (**B**) Scatter plots of the relative change in polysomal association of circRNAs after eIF4A3 downregulation. The *x*- and *y*-axes represent the relative percentage distributions of circRNAs in the polysomal fraction in the undepleted cells and eIF4A3-depleted cells, respectively. The dots corresponding to cGSE1, cCTNNB1 and cZNF609 are depicted in cyan. Three types of cCTNNB1 were observed in our analysis. Statistical analysis was performed using the Wilcoxon signed-rank test. (**C**) Scatter plots showing a correlation between the polysomal association of circRNAs and eIF4A3 dependency. The *x*-axis represents the relative percentage distributions of circRNAs in the polysomal fraction in the undepleted cells. The *y*-axis denotes the relative ratio (on the $\log_2$ scale) of polysomal to subpolysomal level of circRNAs (PS ratio) in eIF4A3-depleted cells to PS ratio in the undepleted cells. **(D, E)** Scatter plots showing the relative change in polysomal association of circRNAs (**D**) or the effect of eIF4A3 downregulation on the PS ratios of circRNAs (**E**) according to its length. **(F, G)** Violin plots for the relative difference in the polysomal association of circRNAs (**F**) or effect of eIF4A3 downregulation on the PS ratios of circRNAs (**G**) according to their types. Statistical analysis was performed using one-way ANOVA with *post hoc* assessment via Tukey's honestly significant difference test. $^{**}P < 0.01$, $^{***}P < 0.001$. **(H, I)** Violin plots for the relative difference in the polysomal association of circRNAs (**H**) or an effect of eIF4A3 downregulation on the PS ratios of circRNAs (**I**) according to the number of EJCs in circRNAs. $^{***}P < 0.001$.

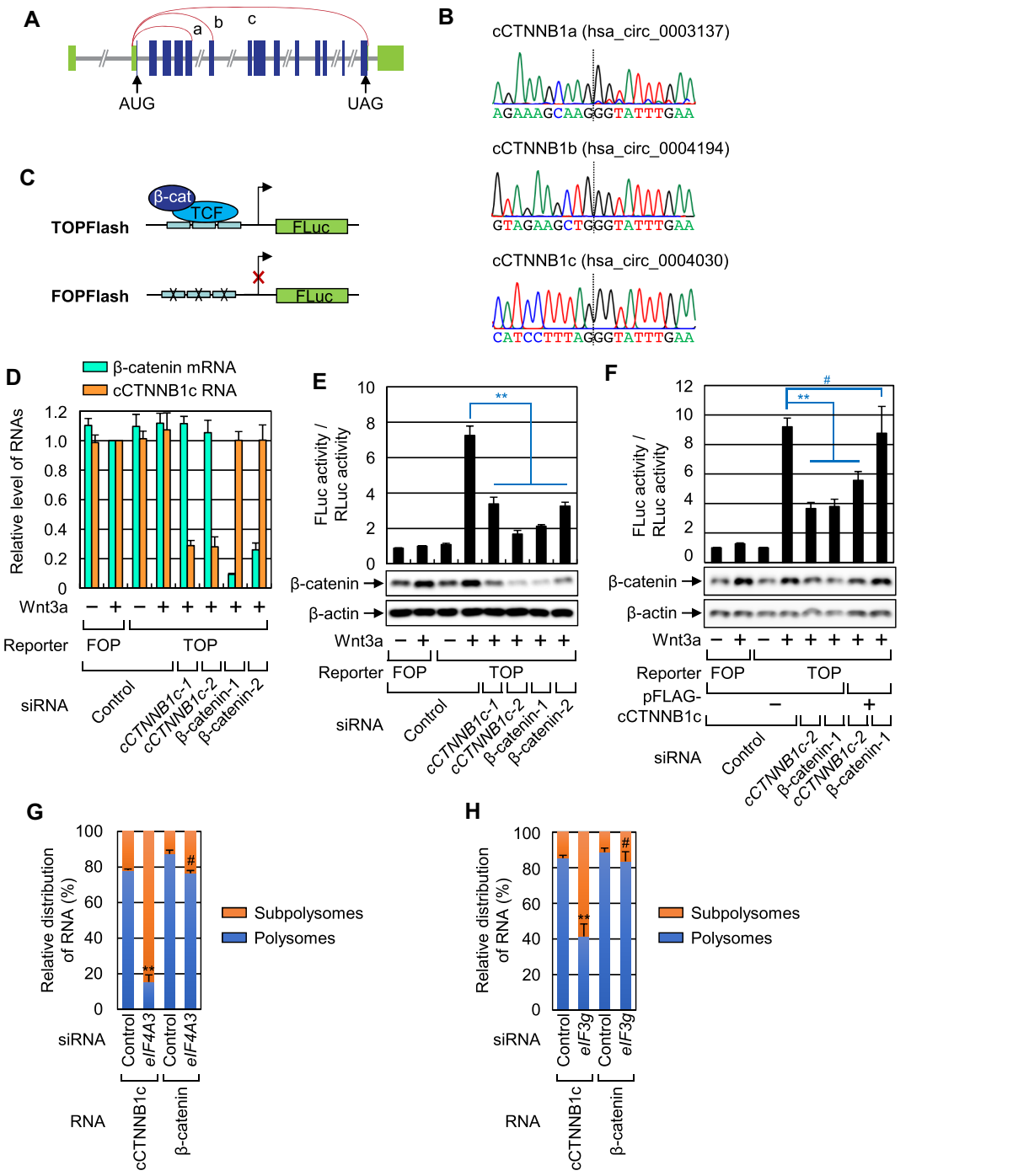

Figure 8. A full-length intact protein can be generated from circRNAs in an eIF4A3-dependent manner. (**A**) The schematic diagram of three isoforms of cCTNNB1 circRNA generated from the β-catenin gene. (**B**) Validation of endogenous cCTNNB1 isoforms. The obtained RT-PCR products shown in Supplementary Figure S9A were subjected to Sanger sequencing. The circRNA-specific exon–exon junctions generated by back-splicing are indicated by vertical dashed lines. (**C**) A schematic diagram of monitoring Wnt/β-catenin signaling using TOPFlash or FOPFlash reporters. An increased amount of β-catenin caused by Wnt3a treatment activates FLuc expression from TOPFlash but not FOPFlash. **(D, E)** The effect of endogenous cCTNNB1c circRNA downregulation on Wnt/β-catenin signaling. HEK293T cells were treated with siRNA specific to cCTNNB1c (#1 or #2) or linear β-catenin mRNA (#1 or #2) that annealed to the 3′UTR of β-catenin mRNA. Two days later, the cells were retransfected with a FLuc reporter [either TOPFlash (TOP) or FOPFlash (FOP)] and a reference plasmid expressing RLuc. The cells were either treated or not treated with 300 ng/ml Wnt3a for 24 h before harvesting. (**D**) Validation of specific downregulation of endogenous cCTNNB1c RNA and linear β-catenin mRNA; $n = 3$. (**E**) The FLuc activities were normalized to RLuc activities. The normalized FLuc levels obtained in the Wnt3a-treated cells transfected with FOPFlash were arbitrarily set to 1.0; $n = 3$; $^{**}P < 0.01$. (**F**) Complementation experiments with pFLAG-cCTNNB1c expressing a circular form of RNA encoding FLAG-cCTNNB1c. As performed in panels **D**, **E**, except that the cells were transiently transfected with pFLAG-cCTNNB1c; $n = 3$; #, not significant; $^{**}P < 0.01$. (**G**) Relative distributions of endogenous cCTNNB1c RNA and its corresponding linear β-catenin mRNA in subpolysomal and polysomal fractions before or after eIF4A3 downregulation; $n = 2$. $^{**}P < 0.01$. (**H**) Relative distributions of endogenous cCTNNB1c RNA and linear β-catenin mRNA in subpolysomal and polysomal fractions before or after eIF3g downregulation; $n = 3$. $^{**}P < 0.01$.

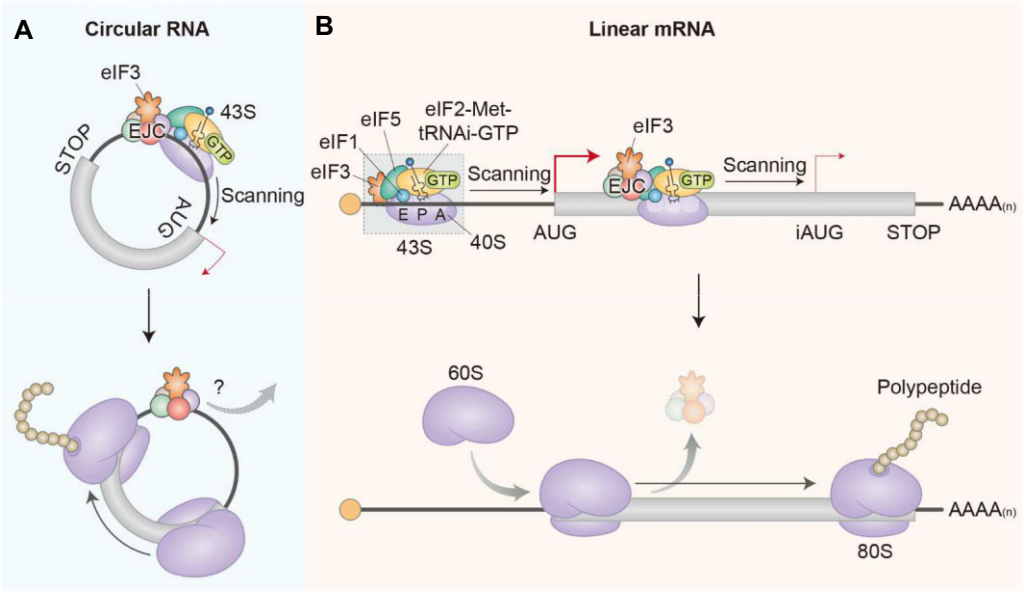

Figure 9. A simplified model illustrating the eIF4A3-driven internal initiation of translation. In this study, we demonstrated that eIF4A3 alone possesses an intrinsic capability to initiate translation internally in an eIF3-dependent manner. Of note, this mode of translation is facilitated by other EJC core components. The relative translation efficiencies of 80S ribosome are indicated by the thickness of red arrows. (**A**) eIF4A3-driven internal initiation of translation in circRNAs. The 40S ribosome associates with circRNA with help of the eIF4A3 (or EJC)–eIF3 interaction and scans for AUG where it forms the 80S ribosome to translate the ORF in circRNA. On termination, the 40S either remains bound to circRNA, displaces the EJC and reinitiates (perhaps repeatedly) translation of the ORF in circRNA or undergoes full ribosome recycling to allow the eIF4A3 (or EJC)–eIF3 complex to mediate repeated internal initiation events. (**B**) eIF4A3-driven internal initiation of translation in linear mRNA. Scanning or elongating ribosomes may displace all EJCs from mRNAs. Owing to this phenomenon, internal initiation driven by eIF4A3 would be suppressed under normal conditions. However, under stressful conditions where the general cap-dependent translation is compromised, the displacement would be inefficient and eIF4A3-mediated internal initiation of translation would become predominant, leading to protein synthesis from a downstream internal AUG (iAUG). See the Discussion section for more details.

promoting efficient recruitment of the eIF3 complex (76). Subsequently, eIF3 recruits a ribosome, consequently leading to the internal translation of circRNAs following a scanning process to search for a translation initiation codon in the proper context.

Our transcriptome-wide analysis revealed that eIF4A3 downregulation reduced the polysomal distribution of circRNAs regardless of the relative position of the back-splicing junction and stop codon (Supplementary Figure S8D, E). These observations suggest that ribosome recruitment may be a rate-limiting step in circRNA translation. Once the 40S ribosome is recruited to the circRNA through the eIF4A3–eIF3 interaction, it begins to scan downstream sequences in search of an AUG in the proper context with help of eIF3 and several other key eIFs. On recognition of AUG, the 60S ribosome joins the 40S ribosome to initiate polypeptide synthesis. After a single round of translation, the 40S ribosome on the translation termination codon may reinitiate the scanning process and be reused for the next round of translation, as observed in ribosome reinitiation on many upstream-ORF-containing mRNAs and circularized mRNAs through a protein-mediated association between the 5′- and 3′-ends (77,78). This way, however, the EJC would be removed, preventing its further use as a primary ribosome-recruitment factor. Further exploration is necessary to fully understand to what extent translation reinitiation on back-spliced exons contributes to translation efficiency on cicrRNAs compared to complete ribosome recycling followed by repeated 'de-novo' internal translation mediated by eIF4A3 (or EJC).

In contrast to circRNAs, for most EJC-associated newly synthesized linear mRNAs, EJCs could be rapidly displaced from mRNAs by elongating ribosomes during the pioneer round of translation (Figure 9B). Accordingly, although the eIF4A3 within EJC deposited onto newly synthesized mRNAs has the potential to drive internal translation, eIF4A3-driven internal initiation is rapidly compromised immediately after the pioneer round of translation. Instead, most EJCs deposited onto newly synthesized mRNAs may participate in increasing the efficiency of general cap-dependent translation by helping eIF3 recruitment to the 5′-cap structure (32–34).

Recent studies have shown that circRNAs are translated via either an IRES (or an IRES-like motif) or an m^6A modification (14–24). In the case of IRES-mediated translation of circRNAs, the insertion of a putative IRES (present within circRNAs) into the intercistronic region of a bicistronic reporter promotes the translation of the second cistron (14–16,18). Remarkably, in the specific case when an IRES is inserted with an endogenous intronic sequence into the intercistronic region, the IRES manifests a strong activity in terms of internal translation (14). A recent study involving a high-throughput circRNA reporter assay system identified tens of thousands of RNA sequences (IRES or IRES-like sequences) that drive circRNA translation (24). The same research group demonstrated that 18S rRNA complementarity and a stem-loop structured RNA element (SuRE) located 40–60 nt upstream of an IRES can promote IRES-dependent translation of circRNAs. Notably, the newly identified IRESs present within the endogenous circRNAs are mostly located near the BSJ. These observations suggest that the functionality of an IRES within endogenous circRNAs depends on a splicing event, supporting our conclusion that eIF4A3 deposited after splicing can drive the internal initiation of translation.

In the case of m^{6}A-mediated internal initiation, m^{6}A residues in circRNAs are directly recognized by YTHDF3 and trigger internal translation by recruiting eIF4G2 (16). Alternatively, m^{6}A residues in circRNAs can be directly recognized by eIF3 for internal initiation (10). Although m^{6}A residues in linear mRNAs are known to recruit eIF3 and drive 5′-end–dependent (and cap-independent) translation (10), eIF3 can also drive internal initiation when it directly associates with a viral IRES (79). Taken together with the results of recent studies showing the direct binding of eIF3 to specific mRNAs (80) and the inhibitory role of eIF3j (considered an eIF3-associated factor rather than a *bona fide* eIF3 component) in circRNA translation (81), the aforementioned observations pique our interest in future investigations to unravel the mechanisms of how the eIF4A3 (or the EJC) interplays with general eIFs, IRES and/or m^{6}A for the internal translation of circRNAs. In particular, given that (i) the absence of detectable levels of eIF1 and eIF5 (both involved in initiation codon selection) in the IP of eIF4A3 (Supplementary Figure S1D), consistent with a previous finding (76), (ii) the preferential enrichment of eIF1 and eIF5 in the IP of eIF3g (Supplementary Figure S1E) and (iii) the inhibition of eIF4A3-driven internal initiation by eIF5 downregulation (Figure 3E), it is plausible that the interaction between eIF4A3 and eIF3g may lead to ribosome recruitment through a mechanism distinct from general cap-dependent ribosome recruitment. Furthermore, considering that eIF4A3 alone can interact with eIF3g, it would be intriguing to explore the molecular and biological impact of the EJC-independent role of eIF4A3 on internal translation.

Although we identified endogenous circRNAs enriched in polysomes in an eIF4A3-dependent manner at the transcriptome level, information on the polypeptide products synthesized from circRNAs in an eIF4A3-dependent manner is currently very limited. In addition, we showed that eIF4A3-driven circRNA translation is resistant to cellular stresses (Figure 6), suggesting that eIF4A3-driven circRNA translation may contribute to the stress response, as does IRES-dependent translation during various cellular stresses (2,9,82). However, because of the lack of information on the polypeptides generated from circRNAs, studies on the underlying mechanisms have limitations. Therefore, to better understand eIF4A3-driven circRNA translation, transcriptomic data should be compared with proteomic data in future studies. Furthermore, considering that the T163 residue of eIF4A3 is phosphorylated by CDK1 and CDK2 in a cell cycle-dependent manner, which leads to the loss of eIF4A3's ability to associate with mRNA (35), posttranslational modifications of eIF4A3 and its helper proteins, such as other EJC components, may contribute to the regulation of eIF4A3-driven circRNA translation. A comprehensive investigation including all these aspects will result in a list of circRNAs and their translation products, and provide valuable insights into the biological and physiological significance of eIF4A3-driven circRNA translation, which has recently been implicated in the regulation of oncogenic pathways through EJC-dependent, cap-independent translation of circSDHAF2 (83).

In conclusion, we provide molecular evidence for a previously unappreciated mode of translation: internal initiation of translation driven by eIF4A3 (and possibly the EJC). These findings elucidate the protein-coding potential of the human transcriptome including circRNAs. In addition, our findings that (i) an intact full-length protein can be generated from circRNA and (ii) eIF4A3-driven internal translation is resistant to cellular stresses (e.g. serum starvation) reveal a new level of complexity in the control of various cellular and biological processes via eIF4A3-driven internal translation of circRNAs as well as linear mRNAs.

Data availability

The circRNA microarray data reported in this paper has been deposited in the GEO Database under accession number GSE131563.

Supplementary data

Supplementary Data are available at NAR Online.

Acknowledgements

We thank Dr. Zefeng Wang for providing pCIRC-FP-IRES-G expressing circRNA, and Dr. John W. Hershey for plasmids encoding GAL4 AD-eIF3 subunits.

Funding

National Research Foundation (NRF) of Korea grant funded by the Korean government (Ministry of Science, ICT and Future Planning; NRF-2015R1A3A2033665, NRF-2018R1A5A1024261, and NRF-2022M3E5F1017965) to Y.K.K; Biotechnology and Biological Sciences Research Council research grant (BB/S006931/1) to N.L. Funding for open access charge: NRF [NRF-2015R1A3A2033665].

Conflict of interest statement

None declared.

References

1. Tahmasebi,S., Khoutorsky,A., Mathews,M.B. and Sonenberg,N. (2018) Translation deregulation in human disease. *Nat. Rev. Mol. Cell Biol.*, **19**, 791–807.
2. Pelletier,J. and Sonenberg,N. (2019) The organizing principles of eukaryotic ribosome recruitment. *Annu. Rev. Biochem.*, **88**, 307–335.
3. Maquat,L.E., Tarn,W.Y. and Isken,O. (2010) The pioneer round of translation: features and functions. *Cell*, **142**, 368–374.
4. Ryu,I. and Kim,Y.K. (2017) Translation initiation mediated by nuclear cap-binding protein complex. *BMB Reports*, **50**, 186–193.
5. Gomes-Duarte,A., Lacerda,R., Menezes,J. and Romão,L. (2018) eIF3: a factor for human health and disease. *RNA Biology*, **15**, 26–34.
6. Wolf,D.A., Lin,Y., Duan,H. and Cheng,Y. (2020) eIF-three to tango: emerging functions of translation initiation factor eIF3 in protein synthesis and disease. *J. Mol. Cell Biol.*, **12**, 403–409.
7. Valášek,L.S., Zeman,J., Wagner,S., Beznosková,P., Pavlíková,Z., Mohammad,M.P., Hronová,V., Herrmannová,A., Hashem,Y. and Gunišová,S. (2017) Embraced by eIF3: structural and functional insights into the roles of eIF3 across the translation cycle. *Nucleic Acids Res.*, **45**, 10948–10968.
8. des Georges,A., Dhote,V., Kuhn,L., Hellen,C.U., Pestova,T.V., Frank,J. and Hashem,Y. (2015) Structure of mammalian eIF3 in the context of the 43S preinitiation complex. *Nature*, **525**, 491–495.
9. Yamamoto,H., Unbehaun,A. and Spahn,C.M.T. (2017) Ribosomal chamber music: toward an understanding of IRES mechanisms. *Trends Biochem. Sci*, **42**, 655–668.

10. Meyer,K.D., Patil,D.P., Zhou,J., Zinoviev,A., Skabkin,M.A., Elemento,O., Pestova,T.V., Qian,S.B. and Jaffrey,S.R. (2015) 5′ UTR m(6)A promotes cap-independent translation. *Cell*, **163**, 999–1010.
11. Chen,L.L. (2016) The biogenesis and emerging roles of circular RNAs. *Nat. Rev. Mol. Cell Biol.*, **17**, 205–211.
12. Zhang,X.O., Wang,H.B., Zhang,Y., Lu,X., Chen,L.L. and Yang,L. (2014) Complementary sequence-mediated exon circularization. *Cell*, **159**, 134–147.
13. Zhou,M., Xiao,M.S., Li,Z. and Huang,C. (2021) New progresses of circular RNA biology: from nuclear export to degradation. *RNA Biology*, **18**, 1365–1373.
14. Legnini,I., Di Timoteo,G., Rossi,F., Morlando,M., Briganti,F., Sthandier,O., Fatica,A., Santini,T., Andronache,A., Wade,M., *et al.* (2017) Circ-ZNF609 is a circular RNA that can Be translated and functions in myogenesis. *Mol. Cell*, **66**, 22–37.
15. Pamudurti,N.R., Bartok,O., Jens,M., Ashwal-Fluss,R., Stottmeister,C., Ruhe,L., Hanan,M., Wyler,E., Perez-Hernandez,D., Ramberger,E., *et al.* (2017) Translation of CcrcRNAs. *Mol. Cell*, **66**, 9–21.
16. Yang,Y., Fan,X., Mao,M., Song,X., Wu,P., Zhang,Y., Jin,Y., Yang,Y., Chen,L.L., Wang,Y., *et al.* (2017) Extensive translation of circular RNAs driven by N6-methyladenosine. *Cell Res.*, **27**, 626–641.
17. Diallo,L.H., Tatin,F., David,F., Godet,A.C., Zamora,A., Prats,A.C., Garmy-Susini,B. and Lacazette,E. (2019) How are circRNAs translated by non-canonical initiation mechanisms?*Biochimie*, **164**, 45–52.
18. Zhang,M., Zhao,K., Xu,X., Yang,Y., Yan,S., Wei,P., Liu,H., Xu,J., Xiao,F., Zhou,H., *et al.* (2018) A peptide encoded by circular form of LINC-PINT suppresses oncogenic transcriptional elongation in glioblastoma. *Nat. Commun.*, **9**, 4475.
19. Wen,S.Y., Qadir,J. and Yang,B.B. (2022) Circular RNA translation: novel protein isoforms and clinical significance. *Trends Mol. Med.*, **28**, 405–420.
20. Wang,Y., Wu,C., Du,Y., Li,Z., Li,M., Hou,P., Shen,Z., Chu,S., Zheng,J. and Bai,J. (2022) Expanding uncapped translation and emerging function of circular RNA in carcinomas and noncarcinomas. *Mol. Cancer*, **21**, 13.
21. Sinha,T., Panigrahi,C., Das,D. and Chandra Panda,A. (2022) Circular RNA translation, a path to hidden proteome. *Wiley Interdiscipl. Rev. RNA*, **13**, e1685.
22. Fan,X., Yang,Y., Chen,C. and Wang,Z. (2022) Pervasive translation of circular RNAs driven by short IRES-like elements. *Nat. Commun.*, **13**, 3751.
23. Liu,C.X. and Chen,L.L. (2021) Expanded regulation of circular RNA translation. *Mol. Cell*, **81**, 4111–4113.
24. Chen,C.K., Cheng,R., Demeter,J., Chen,J., Weingarten-Gabbay,S., Jiang,L., Snyder,M.P., Weissman,J.S., Segal,E., Jackson,P.K., *et al.* (2021) Structured elements drive extensive circular RNA translation. *Mol. Cell*, **81**, 4300–4318.
25. Memczak,S., Jens,M., Elefsinioti,A., Torti,F., Krueger,J., Rybak,A., Maier,L., Mackowiak,S.D., Gregersen,L.H., Munschauer,M., *et al.* (2013) Circular RNAs are a large class of animal RNAs with regulatory potency. *Nature*, **495**, 333–338.
26. Hansen,T.B., Jensen,T.I., Clausen,B.H., Bramsen,J.B., Finsen,B., Damgaard,C.K. and Kjems,J. (2013) Natural RNA circles function as efficient microRNA sponges. *Nature*, **495**, 384–388.
27. Panda,A.C., Grammatikakis,I., Munk,R., Gorospe,M. and Abdelmohsen,K. (2017) Emerging roles and context of circular RNAs. *Wiley Interdiscip. Rev. RNA*, **8**, e1386.
28. Sinha,T., Panigrahi,C., Das,D. and Chandra Panda,A. (2022) Circular RNA translation, a path to hidden proteome. *Wiley Interdiscip. Rev. RNA*, **13**, e1685.
29. Woodward,L.A., Mabin,J.W., Gangras,P. and Singh,G. (2017) The exon junction complex: a lifelong guardian of mRNA fate. *Wiley Interdiscip. Rev. RNA*, **8**, e1411.
30. Le Hir,H., Sauliere,J. and Wang,Z. (2016) The exon junction complex as a node of post-transcriptional networks. *Nat. Rev. Mol. Cell Biol.*, **17**, 41–54.
31. Boehm,V. and Gehring,N.H. (2016) Exon junction complexes: supervising the gene expression assembly line. *Trends in Genetics : TIG*, **32**, 724–735.
32. Nott,A., Le Hir,H. and Moore,M.J. (2004) Splicing enhances translation in mammalian cells: an additional function of the exon junction complex. *Genes Dev.*, **18**, 210–222.
33. Gudikote,J.P., Imam,J.S., Garcia,R.F. and Wilkinson,M.F. (2005) RNA splicing promotes translation and RNA surveillance. *Nat. Struct. Mol. Biol.*, **12**, 801–809.
34. Ma,X.M., Yoon,S.O., Richardson,C.J., Julich,K. and Blenis,J. (2008) SKAR links pre-mRNA splicing to mTOR/S6K1-mediated enhanced translation efficiency of spliced mRNAs. *Cell*, **133**, 303–313.
35. Ryu,I., Won,Y.S., Ha,H., Kim,E., Park,Y., Kim,M.K., Kwon,D.H., Choe,J., Song,H.K., Jung,H., *et al.* (2019) eIF4A3 Phosphorylation by CDKs affects NMD during the cell cycle. *Cell Rep.*, **26**, 2126–2139.
36. Park,O.H., Ha,H., Lee,Y., Boo,S.H., Kwon,D.H., Song,H.K. and Kim,Y.K. (2019) Endoribonucleolytic cleavage of m(6)A-containing RNAs by RNase P/MRP complex. *Mol. Cell*, **74**, 494–507.
37. Choe,J., Ryu,I., Park,O.H., Park,J., Cho,H., Yoo,J.S., Chi,S.W., Kim,M.K., Song,H.K. and Kim,Y.K. (2014) eIF4AIII enhances translation of nuclear cap-binding complex-bound mRNAs by promoting disruption of secondary structures in 5′UTR. *Proc. Natl Acad. Sci. USA*, **111**, E4577–E4586.
38. Choe,J., Oh,N., Park,S., Lee,Y.K., Song,O.K., Locker,N., Chi,S.G. and Kim,Y.K. (2012) Translation initiation on mRNAs bound by nuclear cap-binding protein complex CBP80/20 requires interaction between CBP80/20-dependent translation initiation factor and eukaryotic translation initiation factor 3g. *J. Biol. Chem.*, **287**, 18500–18509.
39. Cho,H., Park,O.H., Park,J., Ryu,I., Kim,J., Ko,J. and Kim,Y.K. (2015) Glucocorticoid receptor interacts with PNRC2 in a ligand-dependent manner to recruit UPF1 for rapid mRNA degradation. *Proc. Natl Acad. Sci. USA*, **112**, E1540–E1549.
40. Park,J., Park,Y., Ryu,I., Choi,M.H., Lee,H.J., Oh,N., Kim,K., Kim,K.M., Choe,J., Lee,C., *et al.* (2017) Misfolded polypeptides are selectively recognized and transported toward aggresomes by a CED complex. *Nat. Commun.*, **8**, 15730.
41. Choe,J., Cho,H., Lee,H.C. and Kim,Y.K. (2010) microRNA/argonaute 2 regulates nonsense-mediated messenger RNA decay. *EMBO Rep.*, **11**, 380–386.
42. Wang,Y. and Wang,Z. (2015) Efficient backsplicing produces translatable circular mRNAs. *RNA*, **21**, 172–179.
43. Korinek,V., Barker,N., Morin,P.J., van Wichen,D., de Weger,R., Kinzler,K.W., Vogelstein,B. and Clevers,H. (1997) Constitutive transcriptional activation by a beta-catenin-TCF complex in APC-/- colon carcinoma. *Science*, **275**, 1784–1787.
44. Wesselhoeft,R.A., Kowalski,P.S. and Anderson,D.G. (2018) Engineering circular RNA for potent and stable translation in eukaryotic cells. *Nat. Commun.*, **9**, 2629.
45. Park,J., Chang,J., Hwang,H.J., Jeong,K., Lee,H.J., Ha,H., Park,Y., Lim,C., Woo,J.S. and Kim,Y.K. (2021) The pioneer round of translation ensures proper targeting of ER and mitochondrial proteins. *Nucleic Acids Res.*, **49**, 12517–12534.
46. Palacios,I.M., Gatfield,D., St Johnston,D. and Izaurralde,E. (2004) An eIF4AIII-containing complex required for mRNA localization and nonsense-mediated mRNA decay. *Nature*, **427**, 753–757.
47. Gehring,N.H., Neu-Yilik,G., Schell,T., Hentze,M.W. and Kulozik,A.E. (2003) Y14 and hUpf3b form an NMD-activating complex. *Mol. Cell*, **11**, 939–949.
48. Kim,Y.K., Furic,L., Desgroseillers,L. and Maquat,L.E. (2005) Mammalian Staufen1 recruits Upf1 to specific mRNA 3′UTRs so as to elicit mRNA decay. *Cell*, **120**, 195–208.
49. Damoc,E., Fraser,C.S., Zhou,M., Videler,H., Mayeur,G.L., Hershey,J.W., Doudna,J.A., Robinson,C.V. and Leary,J.A. (2007) Structural characterization of the human eukaryotic initiation

factor 3 protein complex by mass spectrometry. *Mol. Cell Proteomics. MCP*, **6**, 1135–1146.
50. Pisarev,A.V., Unbehaun,A., Hellen,C.U. and Pestova,T.V. (2007) Assembly and analysis of eukaryotic translation initiation complexes. *Methods Enzymol.*, **430**, 147–177.
51. Cho,H., Kim,K.M., Han,S., Choe,J., Park,S.G., Choi,S.S. and Kim,Y.K. (2012) Staufen1-mediated mRNA decay functions in adipogenesis. *Mol. Cell*, **46**, 495–506.
52. Bustin,S.A., Benes,V., Garson,J.A., Hellemans,J., Huggett,J., Kubista,M., Mueller,R., Nolan,T., Pfaffl,M.W., Shipley,G.L., *et al.* (2009) The MIQE guidelines: minimum information for publication of quantitative real-time PCR experiments. *Clin. Chem.*, **55**, 611–622.
53. Boo,S.H., Ha,H. and Kim,Y.K. (2022) m(1)A and m(6)A modifications function cooperatively to facilitate rapid mRNA degradation. *Cell Rep.*, **40**, 111317.
54. Boo,S.H., Ha,H., Lee,Y., Shin,M.K., Lee,S. and Kim,Y.K. (2022) UPF1 promotes rapid degradation of m(6)A-containing RNAs. *Cell Rep.*, **39**, 110861.
55. Kim,K.M., Cho,H., Choi,K., Kim,J., Kim,B.W., Ko,Y.G., Jang,S.K. and Kim,Y.K. (2009) A new MIF4G domain-containing protein, CTIF, directs nuclear cap-binding protein CBP80/20-dependent translation. *Genes Dev.*, **23**, 2033–2045.
56. Alexandrov,A., Colognori,D. and Steitz,J.A. (2011) Human eIF4AIII interacts with an eIF4G-like partner, NOM1, revealing an evolutionarily conserved function outside the exon junction complex. *Genes Dev.*, **25**, 1078–1090.
57. Li,Q., Imataka,H., Morino,S., Rogers,G.W. Jr, Richter-Cook,N.J., Merrick,W.C. and Sonenberg,N. (1999) Eukaryotic translation initiation factor 4AIII (eIF4AIII) is functionally distinct from eIF4AI and eIF4AII. *Mol. Cell. Biol.*, **19**, 7336–7346.
58. Fredriksson,S., Gullberg,M., Jarvius,J., Olsson,C., Pietras,K., Gústafsdóttir,S.M., Ostman,A. and Landegren,U. (2002) Protein detection using proximity-dependent DNA ligation assays. *Nat. Biotechnol.*, **20**, 473–477.
59. Andersen,C.B., Ballut,L., Johansen,J.S., Chamieh,H., Nielsen,K.H., Oliveira,C.L., Pedersen,J.S., Seraphin,B., Le Hir,H. and Andersen,G.R. (2006) Structure of the exon junction core complex with a trapped DEAD-box ATPase bound to RNA. *Science*, **313**, 1968–1972.
60. Bono,F., Ebert,J., Lorentzen,E. and Conti,E. (2006) The crystal structure of the exon junction complex reveals how it maintains a stable grip on mRNA. *Cell*, **126**, 713–725.
61. Trcek,T., Sato,H., Singer,R.H. and Maquat,L.E. (2013) Temporal and spatial characterization of nonsense-mediated mRNA decay. *Genes Dev.*, **27**, 541–551.
62. Gehring,N.H., Lamprinaki,S., Hentze,M.W. and Kulozik,A.E. (2009) The hierarchy of exon-junction complex assembly by the spliceosome explains key features of mammalian nonsense-mediated mRNA decay. *PLoS Biol.*, **7**, e1000120.
63. Shibuya,T., Tange,T.O., Stroupe,M.E. and Moore,M.J. (2006) Mutational analysis of human eIF4AIII identifies regions necessary for exon junction complex formation and nonsense-mediated mRNA decay. *RNA*, **12**, 360–374.
64. Le Hir,H., Izaurralde,E., Maquat,L.E. and Moore,M.J. (2000) The spliceosome deposits multiple proteins 20-24 nucleotides upstream of mRNA exon-exon junctions. *EMBO J.*, **19**, 6860–6869.
65. Xin,R., Gao,Y., Gao,Y., Wang,R., Kadash-Edmondson,K.E., Liu,B., Wang,Y., Lin,L. and Xing,Y. (2021) isoCirc catalogs full-length circular RNA isoforms in human transcriptomes. *Nat. Commun.*, **12**, 266.
66. Ho-Xuan,H., Glažar,P., Latini,C., Heizler,K., Haase,J., Hett,R., Anders,M., Weichmann,F., Bruckmann,A. and Van den Berg,D. (2020) Comprehensive analysis of translation from overexpressed circular RNAs reveals pervasive translation from linear transcripts. *Nucleic Acids Res.*, **48**, 10368–10382.
67. Chuang,T.W., Lee,K.M., Lou,Y.C., Lu,C.C. and Tarn,W.Y. (2016) A point mutation in the exon junction complex factor Y14 disrupts its function in mRNA cap binding and translation enhancement. *J. Biol. Chem.*, **291**, 8565–8574.
68. Lee,H.C., Choe,J., Chi,S.G. and Kim,Y.K. (2009) Exon junction complex enhances translation of spliced mRNAs at multiple steps. *Biochem. Biophys. Res. Commun.*, **384**, 334–340.
69. Li,S., Teng,S., Xu,J., Su,G., Zhang,Y., Zhao,J., Zhang,S., Wang,H., Qin,W., Lu,Z.J., *et al.* (2019) Microarray is an efficient tool for circRNA profiling. *Brief Bioinform*, **20**, 1420–1433.
70. Nusse,R. and Clevers,H. (2017) Wnt/beta-catenin signaling, disease, and emerging therapeutic modalities. *Cell*, **169**, 985–999.
71. Liang,W.C., Wong,C.W., Liang,P.P., Shi,M., Cao,Y., Rao,S.T., Tsui,S.K., Waye,M.M., Zhang,Q., Fu,W.M., *et al.* (2019) Translation of the circular RNA circbeta-catenin promotes liver cancer cell growth through activation of the Wnt pathway. *Genome Biol.*, **20**, 84.
72. Miller,J.R., Hocking,A.M., Brown,J.D. and Moon,R.T. (1999) Mechanism and function of signal transduction by the wnt/beta-catenin and wnt/Ca2+ pathways. *Oncogene*, **18**, 7860–7872.
73. Buchert,M., Athineos,D., Abud,H.E., Burke,Z.D., Faux,M.C., Samuel,M.S., Jarnicki,A.G., Winbanks,C.E., Newton,I.P., Meniel,V.S., *et al.* (2010) Genetic dissection of differential signaling threshold requirements for the Wnt/beta-catenin pathway in vivo. *PLos Genet.*, **6**, e1000816.
74. Wu,X., Tu,X., Joeng,K.S., Hilton,M.J., Williams,D.A. and Long,F. (2008) Rac1 activation controls nuclear localization of beta-catenin during canonical Wnt signaling. *Cell*, **133**, 340–353.
75. Bakker,E.R., Hoekstra,E., Franken,P.F., Helvensteijn,W., van Deurzen,C.H., van Veelen,W., Kuipers,E.J. and Smits,R. (2013) β-catenin signaling dosage dictates tissue-specific tumor predisposition in Apc-driven cancer. *Oncogene*, **32**, 4579–4585.
76. Chazal,P.E., Daguenet,E., Wendling,C., Ulryck,N., Tomasetto,C., Sargueil,B. and Le Hir,H. (2013) EJC core component MLN51 interacts with eIF3 and activates translation. *Proc. Natl Acad. Sci. USA*, **110**, 5903–5908.
77. Hellen,C.U.T. (2018) Translation termination and ribosome recycling in eukaryotes. *Cold Spring Harb. Perspect. Biol.*, **10**, a032656.
78. Hronová,V., Mohammad,M.P., Wagner,S., Pánek,J., Gunišová,S., Zeman,J., Poncová,K. and Valášek,L.S. (2017) Does eIF3 promote reinitiation after translation of short upstream ORFs also in mammalian cells?*RNA Biology*, **14**, 1660–1667.
79. Jackson,R.J., Hellen,C.U. and Pestova,T.V. (2010) The mechanism of eukaryotic translation initiation and principles of its regulation. *Nat. Rev. Mol. Cell Biol.*, **11**, 113–127.
80. Lee,A.S., Kranzusch,P.J. and Cate,J.H. (2015) eIF3 targets cell-proliferation messenger RNAs for translational activation or repression. *Nature*, **522**, 111–114.
81. Song,Z., Lin,J., Su,R., Ji,Y., Jia,R., Li,S., Shan,G. and Huang,C. (2022) eIF3j inhibits translation of a subset of circular RNAs in eukaryotic cells. *Nucleic Acids Res.*, **50**, 11529–11549.
82. Shatsky,I.N., Terenin,I.M., Smirnova,V.V. and Andreev,D.E. (2018) Cap-independent translation: what's in a name?*Trends Biochem. Sci*, **43**, 882–895.
83. Lin,H.H., Chang,C.Y., Huang,Y.R., Shen,C.H., Wu,Y.C., Chang,K.L., Lee,Y.C., Lin,Y.C., Ting,W.C., Chien,H.J., *et al.* (2023) Exon junction complex mediates the cap-independent translation of circular RNA. *Mol. Cancer Res.*, https://doi.org/10.1158/1541-7786.MCR-22-0877.

Received: November 4, 2022. **Revised:** August 30, 2023. **Editorial Decision:** August 31, 2023. **Accepted:** September 8, 2023